FINAL REPORT

GYRO NOISE STUDY PROGRAM

21367-FR

G. M. Kraus

March 1970

Prepared Under

JPL Contract No. 952575

by

Honeywell Inc.
Aerospace Division
Minneapolis, Minnesota

Final Report

GYRO NOISE STUDY PROGRAM

21367-FR

G.M. Kraus

March 1970

This work was performed for the Jet Propulsion Laboratory, California Institute of Technology, sponsored by the National Aeronautics and Space Administration under Contract NAS 7-100.

Prepared Under

JPL Contract No. 952575

by

Honeywell Inc.
Aerospace Division
Minneapolis, Minnesota

CONTENTS

ILLUSTRATIONS

TABLES

SECTION I
SUMMARY AND INTRODUCTION

SUMMARY

This final report is submitted in accordance with JPL Contract No. 952575. This program was to determine the most effective means of reducing noise on the output signal of a floated, rate integrating, single-degree-of-freedom gyro. The program was both theoretical and experimental in nature; design studies were conducted, and hardware was fabricated and tested to substantiate the results of the studies. For this program the noise requirement was 1.0 deg/hr peak to peak for that noise between 0.01 and 25 Hz measured while the gyro was operating in a 25-Hz loop. The basic design of the gyro was that of a Honeywell Model GG334S.

Results of this program show that low-frequency gyro noise is caused primarily by turbulent windage torques within the gimbal associated with the rotating wheel. Program results also show that these windage torques can be changed from a turbulent to laminar condition by incorporating suitably spaced windage shrouds, resulting in an overall gyro noise reduction of approximately 6:1. This noise reduction, incorporated in the GG334S with no additional changes, produces levels of 1.6 deg/hr peak-to-peak noise based on tests conducted at the gimbal assembly level. The fabrication and test of a gyro incorporating these shrouds, plus a factor of two increase in angular momentum, provided the means of attaining less than 1.0 deg/hr peak to peak or approximately 0.16 deg/hr rms noise over 25 Hz.

INTRODUCTION

Results of extensive gyro noise testing conducted at Honeywell on gyros similar to the GG334S serve as background to this program. This background testing gave strong indications of the probable source of gyro noise, thereby allowing this program to (1) verify the source of noise and study the mechanism, and (2) develop means to significantly reduce this noise. For continuity and reference purposes, a summary of this background testing is presented in Section II. Results of this gyro noise reduction study are presented in Section III, with conclusions and recommendations presented in Sections IV and V.

SECTION II
GYRO NOISE/PROGRAM BACKGROUND

The use of an integrating rate gyroscope in an electrically closed loop to measure rate is a well established technique. As shown in Figure 1, the integrating gyro consists of a synchronous spinmotor to develop the required momentum vector, $\bar{H}$. The input rate vector, $\bar{\omega}$, acting on the momentum vector, $\bar{H} x \bar{\omega}$, produces a torque on the fluid-damped gimbal, resulting in a gimbal rate $\dot{\theta}g$. This gimbal rate results in a gimbal angular displacement which is, in turn, sensed by the pickoff (essentially an angular phase-sensitive differential transformer) to produce a phase-sensitive, a-c voltage that is amplitude modulated by the gimbal position.

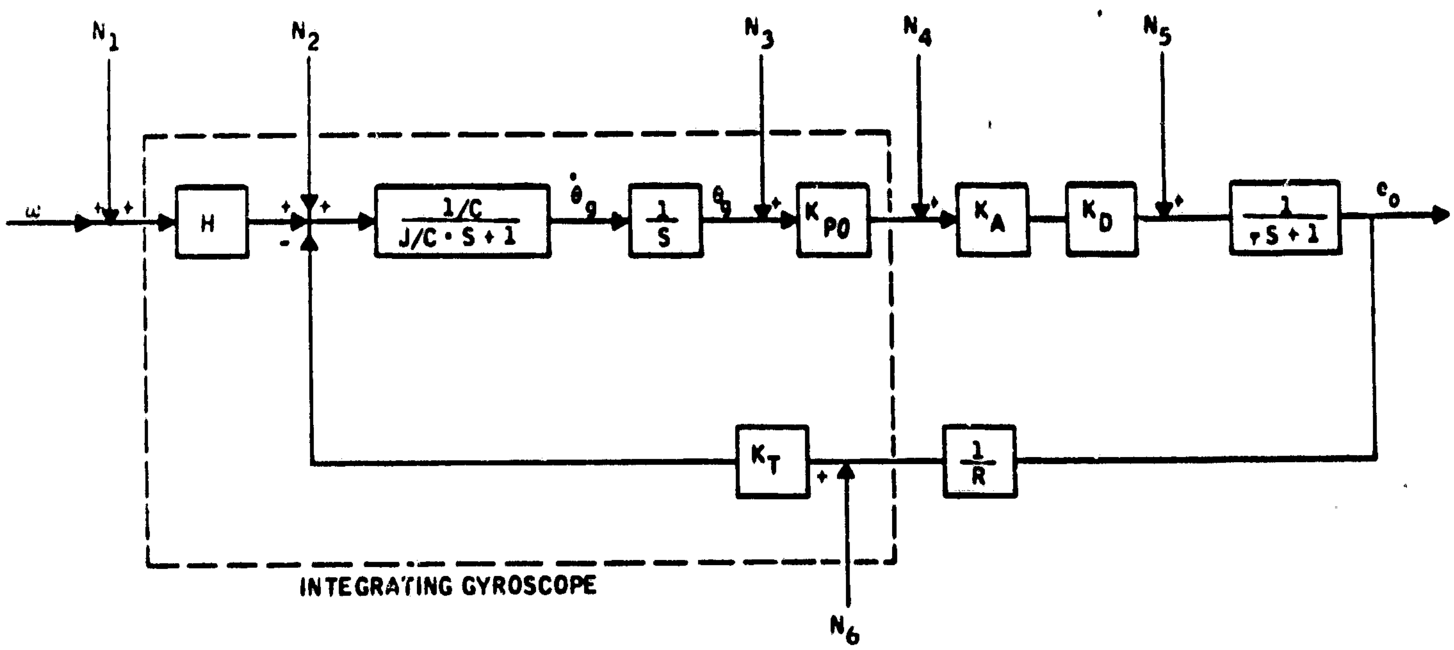

Figure 1. Rate Gyro Loop with Primary Noise Source Locations Indicated

The gyroscope output signal, an amplitude-modulated carrier, is generally sensed and amplified by an a-c preamplifier prior to the demodulation by the reference carrier signal. The demodulator output signal is usually ripple filtered and d-c amplified to form a torquer current signal that is fed through a series readout resistor and the torquer winding. This torquer current results in a torque applied to the gimbal to counterbalance the gyroscopic torque resulting from the input rate.

The output of the demodulator-amplifier is an accurate measure of the input rate since the accuracy-limiting components are the feedback series resistor and torquer scale factor, both of which can be held to good precision.

Theoretically, if the input rate is zero, the output voltage should also be zero. In practice, this is not possible and the resulting output contains spurious signals in the frequency range from 0 to several Hz, which corrupt any precision low-rate measurements. The following paragraphs delineate the apparent noise sources in the low- to medium-frequency range along with a discussion of their probable relative effect.

APPARENT GYRO NOISE SOURCES

Apparent noise sources N_1 through N_6 are shown as additive noise in Figure 1 at approximate locations in the rate loop where they are likely to occur.

- N_1 is actual undesired input rate motion caused by angular or rectilinear motion of the gyro test stand.
- N_2 is mechanical noise resulting in actual gimbal motion. This can be caused by spinmotor hunt or changes in load torque resulting in spinmotor accelerations about the spin axis, which couple into the output axis due to nonperpendicularities. This gimbal motion could also be caused by convection motion in the damping fluid or changes in any electromagnetic coupling torque acting on the gimbal.
- N_3 is noise caused by electrical coupling to the pickoff by spinmotor excitation, rotating poles of the hysteresis motor, or other electrical sources.
- N_4 is noise associated with the a-c amplifier and depends on gain and bandwidth. Characteristics of this source are those typically associated with semiconductor electronics.
- N_5 is the noise contribution of the demodulation process which result from both switching assymetries and foldback effects.
- N_6 is the noise caused by electrical coupling to the torquer coils by spinmotor or other excitations.

The voltage output transfer characteristics for these noise sources are approximately as follows:

$$\frac{\ell o}{N_1} = \frac{H/C,\ K_{po},\ K_T}{S + \frac{1}{C} \cdot \frac{1}{R} \cdot K_{po} \cdot K_A \cdot K_T} = \frac{H/C \cdot K_{po} \cdot K_A}{S + \alpha}$$

$$\frac{\ell o}{N_2} = \frac{1/C \cdot K_{po} \cdot K_A}{S + \alpha}$$

$$\frac{\ell o}{N_3} = \frac{S \cdot K_{po} \cdot K_A}{S + \alpha}$$

$$\frac{\ell o}{N_4} = \frac{S \cdot K_A}{S + \alpha}$$

$$\frac{\ell o}{N_5} = \frac{S}{S + \alpha}$$

$$\frac{\ell o}{N_6} = \frac{1/C \cdot K_T \cdot K_{po} \cdot K_A}{S + \alpha}$$

Noise sources N_1, N_2, and N_6 would be acted on by the loop dynamics and, as such, are attenuated at higher frequencies. The remainder of the noise sources is located in the forward-loop components and, as such, arises after the integration effect of the gyroscope and is highpassed to the output by the loop dynamics.

RELATIVE EFFECT OF NOISE SOURCES

Investigations have been conducted at Honeywell in an attempt to isolate the previously listed noise sources, identify the character of each, and establish techniques to eliminate or reduce each to a tolerable level. Of particular interest are the results of investigations conducted on the GG334A gyro in noise measurement and reduction. The GG334A is basically similar in design to the GG334S and GG159E, especially with respect to the gas bearing spin-motor configuration. Thus, concusions on noise effects are applicable.

Key pieces of information noted on GG334A noise measurement at the gyro level are:

- With the gyro operating in a 25-Hz analog loop a reduction in rate noise of approximately 10:1 can be achieved by turning off the spinmotor, leaving all other parameters constant (Table I).

- Reducing the electrical gain of the system by providing increased mechanical gain does not result in a significant noise reduction.

Table I. GG334A Gyro Noise versus Bandwidth (25 Hz Loop)

Bandwidth, Hz	Noise Degrees [illegible] rms	
	Motor On	[illegible] r Off
0-25	1.35	0.[illegible]35
0-10	0.54	0.102
0.5	0.19	0.07

Turning off the gyro spinmotor eliminated noise source N_1 by reducing H to zero. Other sources affected were N_2, N_3, and N_6, since they depend on various electromagnetic coupling effects or mechanical motions of the gimbal related to a rotating spinmotor. Separate tests, conducted in an effort to eliminate test stand motion or seismic inputs, have further shown that the effect of N_1 does not appear to be the limiting factor. Transportation of test units from one geographical location to another indicates that spurious rate inputs usually account for approximately 15% of the total rms noise on the GG334A and can be lowered by proper choice of test site or positioning of gyro axes. Noise sources N_4 and N_5 remained unchanged by turning off the spinmotor; it is concluded that their total input is, at worst, equal to the gyro noise with the motor off. Based on this test, noise sources N_2, N_3, and N_6 appear to be the prime contributors.

Reducing the electrical gain of the system was accomplished by fabricating gyros with lower output axis damping, thereby attaining a second-order system nearly critically damped and with less amplifier gain (K_A) required. The magnitude of reduction on damping was 10, thereby allowing a substantial reduction in electrical gain. As stated earlier, a significant reduction in noise did not follow. Referring to the transfer functions of the various noise sources, the following conclusions can be made:

- Noise sources N_3 and N_4 should have been significantly reduced. Noise sources N_1, N_2, N_5, and N_6 were not affected by this change because either K_A is not part of the expression or it appears in conjunction with $1/C$, thus nullifying any effect, since $K_A \cdot 1/C$ remained unchanged.

- Based on these tests and observations, noise sources N_2 and N_6 could not be eliminated as major noise contributors. Noise source N_6 is coupling induced and cannot be eliminated (based on the motor-off tests), since the motor excitation could be the mechanism.

- One additional test, measuring rate loop noise during spinmotor rundown, showed that noise decreased gradually and was proportional to wheel speed, whether the motor was in a magnetized or demagnetized state. This test eliminated the possibility of spinmotor electromagnetic coupling to the torquer coils (N_6) as being a primary noise source.

- Thus, these tests and observations indicate that the primary source of gyro noise is of a mechanical nature (N_2), resulting in actual gimbal motion. Noise source, N_2, encompasses such mechanically induced torques as spinmotor hunt, convection currents in the damping fluid, pivot/jewel friction, and motor induced torques.

Further investigations into the nature of the noise source N_2 provided indications that the most likely mechanical noise was that due to windage. First, analysis showed that approximately 400 dyne-cm of motor windage torques were possible within the GG334 gimbal. Since such a large prime torque was available, it was reasonable to expect a noise torque of at least 10 dyne-cm (10 deg/hr) to appear in the frequency range of interest.

Secondly, gyro experiments showed that increasing the density of the gimbal gas resulted in an almost direct increase in gyro noise. The increase in density was accomplished by utilizing air instead of the normal hydrogen for the gimbal fill gas.

In summary, the major source of noise in the 0- to 25-Hz range of the GG334/GG159-type of gas-bearing gyro appears to be mechanical, caused by turbulence within the gimbal resulting from the rotating spinmotor. In addition, complete removal of this noise source, if possible, could result in a drastic reduction in gyro noise as evidenced by the motor-off noise level.

SECTION III

GYRO NOISE REDUCTION TECHNICAL DISCUSSION

This section describes the work performed on this program and the results obtained. The program consisted of three basic tasks. For Task I, first baseline gyro testing was performed by JPL on a GG334S gyro and the data furnished to Honeywell for analysis. The purpose of this phase was to substantiate that the same mechanism is responsible for the GG334S noise as for the noise measured on similar gyros. This is described in Section II. Task II consisted of experimental and analytical studies to obtain a detailed knowledge of the noise mechanism and to develop means of eliminating or reducing its effect. Finally, in Task III gyro hardware was designed and fabricated using the techniques and guidelines established previously to obtain significant noise reduction. The hardware fabricated and tested ranged from motor and gimbal assemblies to a complete gyro.

BASELINE GYRO TESTING

GG334S S/N A-4 was tested at JPL to determine the noise characteristics in a 25-Hz loop. Data taken included rms and peak-to-peak readings of the torquer rebalance signal for both the motor-on and motor-off conditions. In addition, a magnetic tape recording of the analog signal for these cases along with Power Spectral Density (PSD) curves for the motor-on case was determined.

The peak-to-peak and rms noise data substantiated the dramatic reduction in noise achievable by turning off the gyro spinmotor. The relative reduction in noise motor-on to motor-off on a peak-to-peak and rms basis was 7:1 and 13:1, respectively. This is in close agreement with the results of previous tests on similar gyros as outlined in Section II.

Correlation between the absolute values of gyro noise measured at JPL and at Honeywell was clouded by the presence of a considerable 60-Hz signal on the magnetic tape data. However, similarity of the GG334S gyro with that of the gyros used in previous noise testing along with the same motor-on to motor-off noise reduction phenomenon offers sufficient verification that the conclusions arrived at in Section II are applicable to the GG334S and to this program. These conclusions are that:

- The major source of noise in the 0- to 25-Hz range of the GG334/GG159-type gyro appears to be mechanical, caused by turbulence within the gimbal resulting from the rotating spinmotor.

- Complete removal of this noise source, if possible, could result in a drastic reduction in gyro noise (i.e., a factor of 7:1) as evidenced by the motor-off noise level.

EXPERIMENTAL AND ANALYTICAL STUDIES OF GAS TURBULENCE WITHIN THE GG334 GIMBAL

This phase of the program covered work accomplished in two major areas. First, experiments and analyses were conducted on actual gyro hardware to determine the rough magnitude of gas turbulence within the gimbal and to verify that this turbulence was sufficient to produce the noise measured at the gyro level. Secondly, experiments were conducted on a 4X scale model of the GG334S gimbal to obtain detailed measurements of turbulence and develop means to reduce or eliminate its effect.

Gimbal Experiments and Analyses

The gimbal and spinmotor assembly used for these tests was that of a GG334A gyro. This vehicle was chosen because of its availability and extremely close similarity to the GG334S (differing in configuration only in rotor radius and inertia). A hot-wire anemometer was calibrated and installed in the gimbal as shown in Figure 2.

Velocity measurements were made at six locations within the gimbal with the rotor spinning at a rated 24,000 rpm in air. The mean velocities at these locations ranged from 5 ft/sec in the corner areas of the gimbal to 16 ft/sec in the immediate vicinity of the rotor. These velocities are between 1/30 and 1/10 of the maximum rotor surface speed of 160 ft/sec.

In addition to the mean velocities measured, fluctuations in these velocities on the order of 50 to 85% were measured at all six locations. In the corner regions of the gimbal the mean velocity measurement was independent of the hot-wire orientation and typical of a turbulent and separated flow field. To get a measurement of the frequency content of the velocity fluctuations, the anemometer signal was filtered over various ranges out to a bandwidth of 1 KHz using a Krohn-Hite filter. On a peak-to-peak basis, most of the noise is below 50 Hz.

The gimbal assembly was then filled with the normal Hydrogen-Helium gas used on the GG334S, and the velocity measurements were repeated at one representative location. The mean velocity in hydrogen was within 10% of the mean velocity in air at the same location, and the fluctuations in velocity were in agreement with those measured in air. High-speed analog recorder traces of the gas velocities were virtually identical for hydrogen and air.

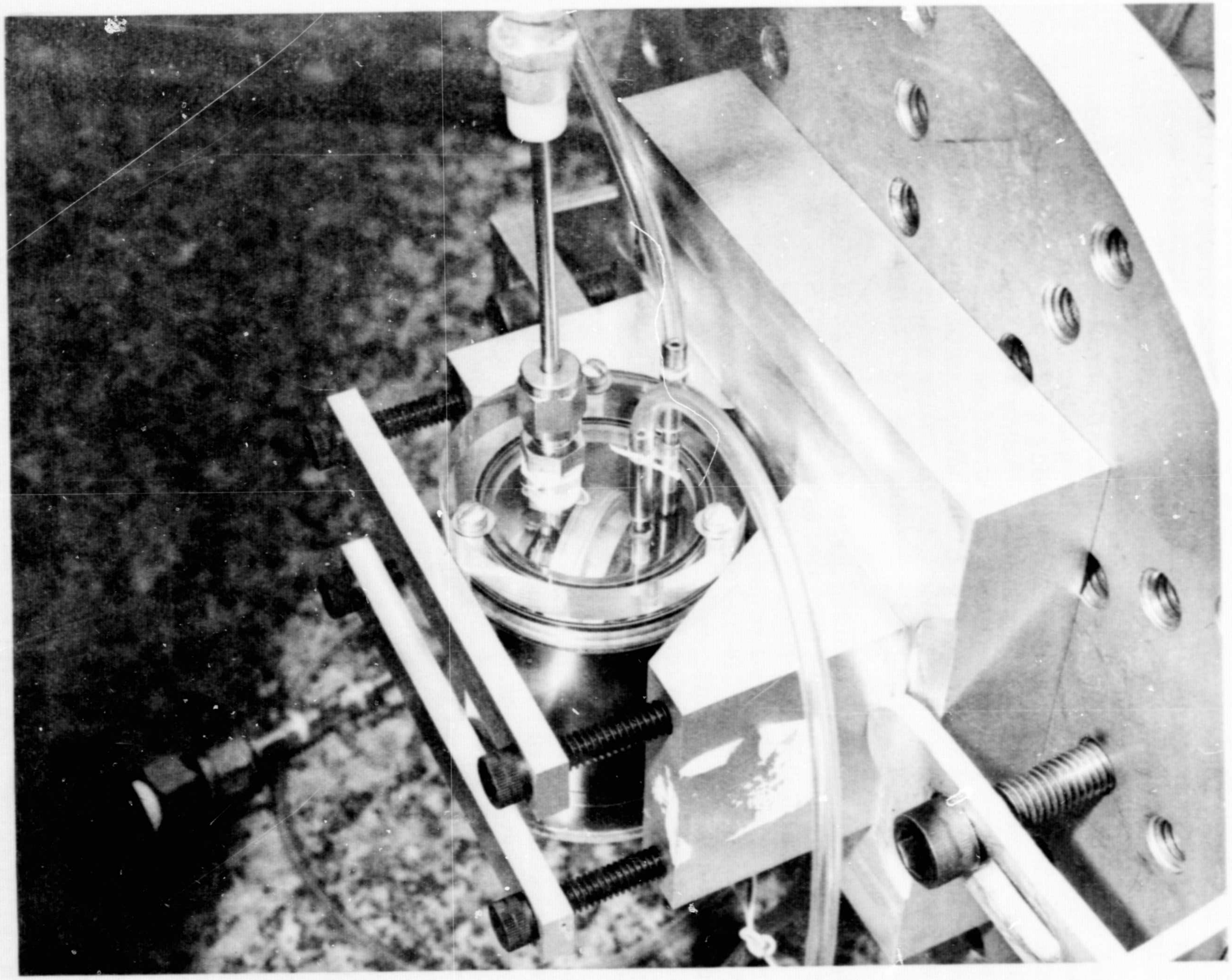

Figure 2. GG334 Gimbal with Hot Wire Anemometer Probe

Appendix A presents analyses of the possible magnitude of torques associated with these measurements. These analyses indicate that error torques on the order of 5 dyne-cm (10 deg/hr on the GG334S) could easily be attributed to gas turbulence within the gimbal.

The analog signal of the hot-wire anemometer was also sampled and processed by digital computer to obtain a PSD estimate of the gas turbulence within the gimbal. The motor was normally excited and running at 24, 000 rpm in the Hydrogen-Helium gas used in the GG334S gimbal. Since any gimbal-associated noise (such as the turbulence under investigation) would be acted on by the gyro loop characteristics as if it were a rate input, the anemometer signal was passed through a first-order R-C filter with a 0- to 25-Hz bandwidth to simulate the effects of the gyro loop. Figure 3 presents the PSD estimate.

For comparison, a PSD estimate of GG334S gyro noise in a 25-Hz loop is presented in Figure 4. This PSD run was taken at JPL on GG334S S/N A-4. While it may be unreasonable to expect good correlation on noise data taken on two different test vehicles using two separate computational methods, there are some similarities. In the 1- to 10-Hz band of Figure 3, two frequency spikes appear at 4. 5 and 9. 5 Hz, while on the gyro data of Figure 4, spikes appear at 3 and 10 Hz. Above 10 Hz on both figures, where the bulk of the noise is located, the PSD is indicative of a random noise signal passed through a 25-Hz lowpass filter.

In summary, the measurements and analysis of gas turbulence indicate that the levels of torque available from turbulent flow are more than sufficient to cause the gyro noise torques present. Also, the PSD curve indicates that the frequency content of the gas turbulence is in the range to be passed by the gyro loop characteristics and is in general agreement with the gyro PSD estimate.

Construction and Test of 4X Scale Model

A 4X scale model of the GG334S gimbal-motor assembly was fabricated and tested. This model, operating in air, allowed a reduction in rotor speed by a factor of 111, or approximately 3. 6 rps as compared to the 400-rps speed for the GG334S motor. A derivation of the rotor speed of the 4X scale model is presented in Appendix II.

Hot-wire anemometer measurements were taken at five locations in the model. Figure 5 shows a cutaway of the model and the probe locations. Table II is a list of the data taken. The data are tabulated both in mean velocity and in Δ velocity which corresponds to the peak-to-peak fluctuations in velocity as measured with an oscilloscope. As with the preliminary data taken on the instrumented GG334A gimbal, turbulent conditions existed throughout the model with fluctuations in the mean velocities ranging from 10% to greater than 100%. The close agreement between the scaled model data and that of

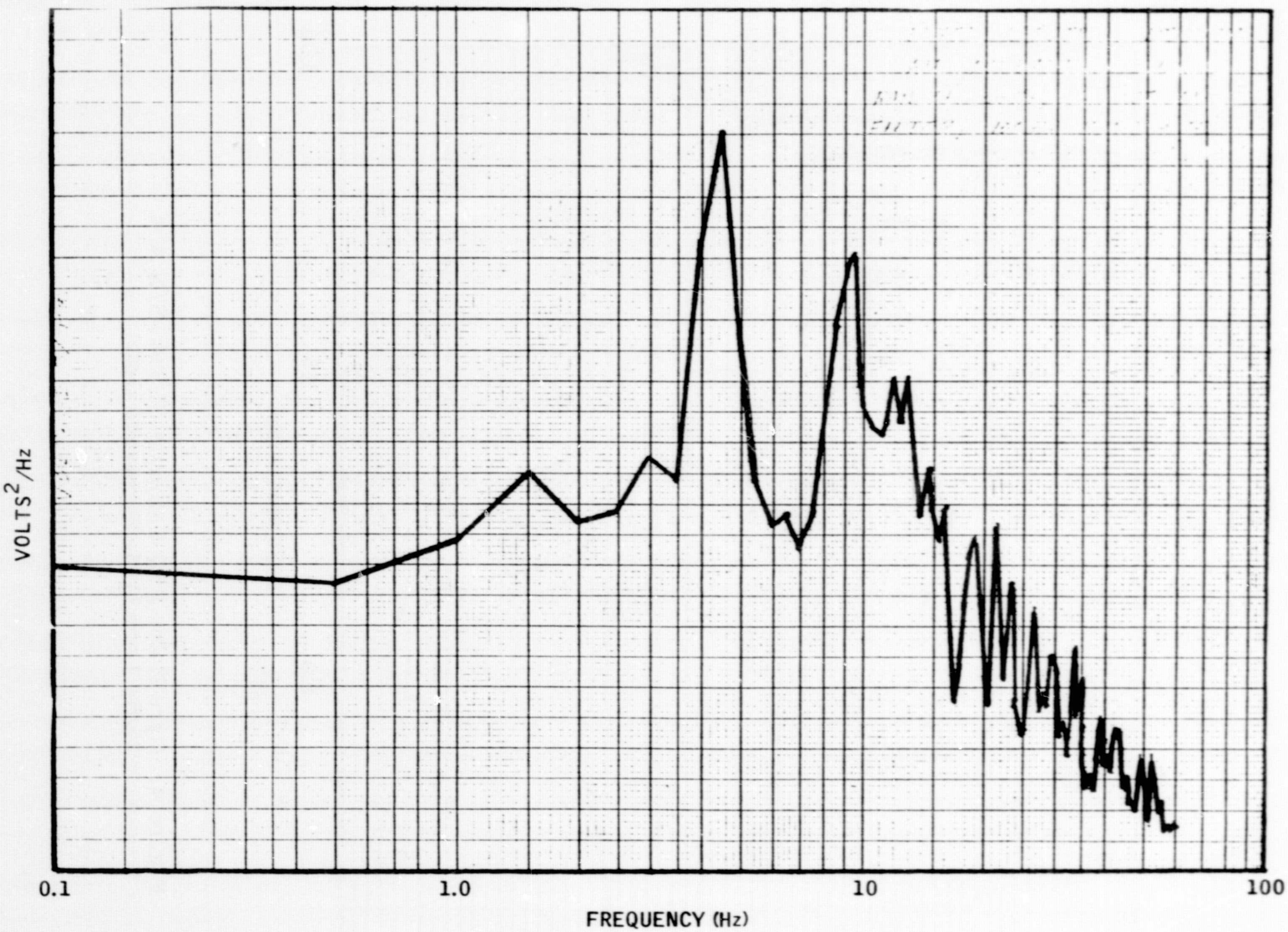

Figure 3. Gimbal Gas Flow PSD Estimate

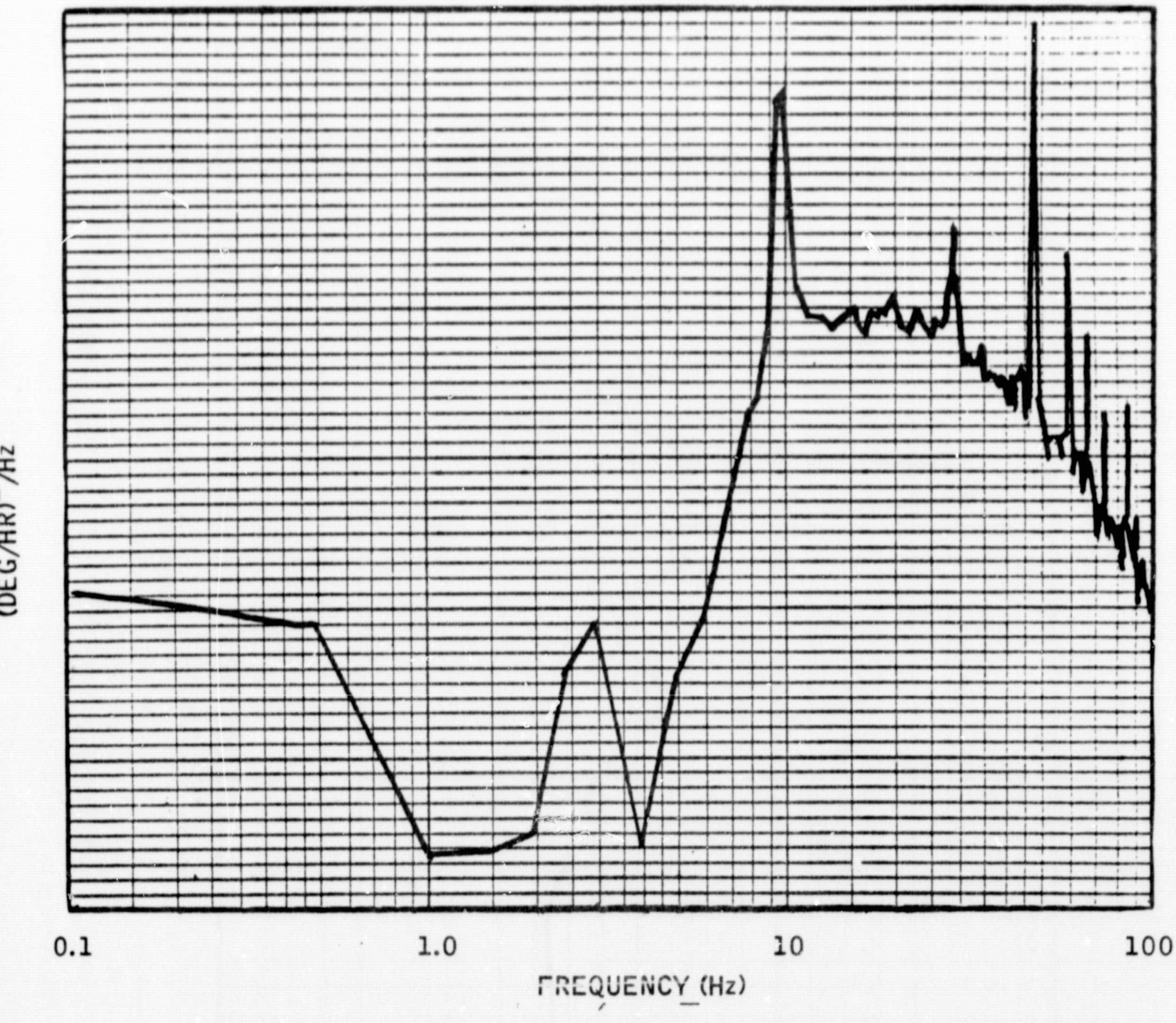

Figure 4. Gyro Noise PSD Estimate GG334S S/N A-4
25 Hz Loop (JPL Furnished Data)

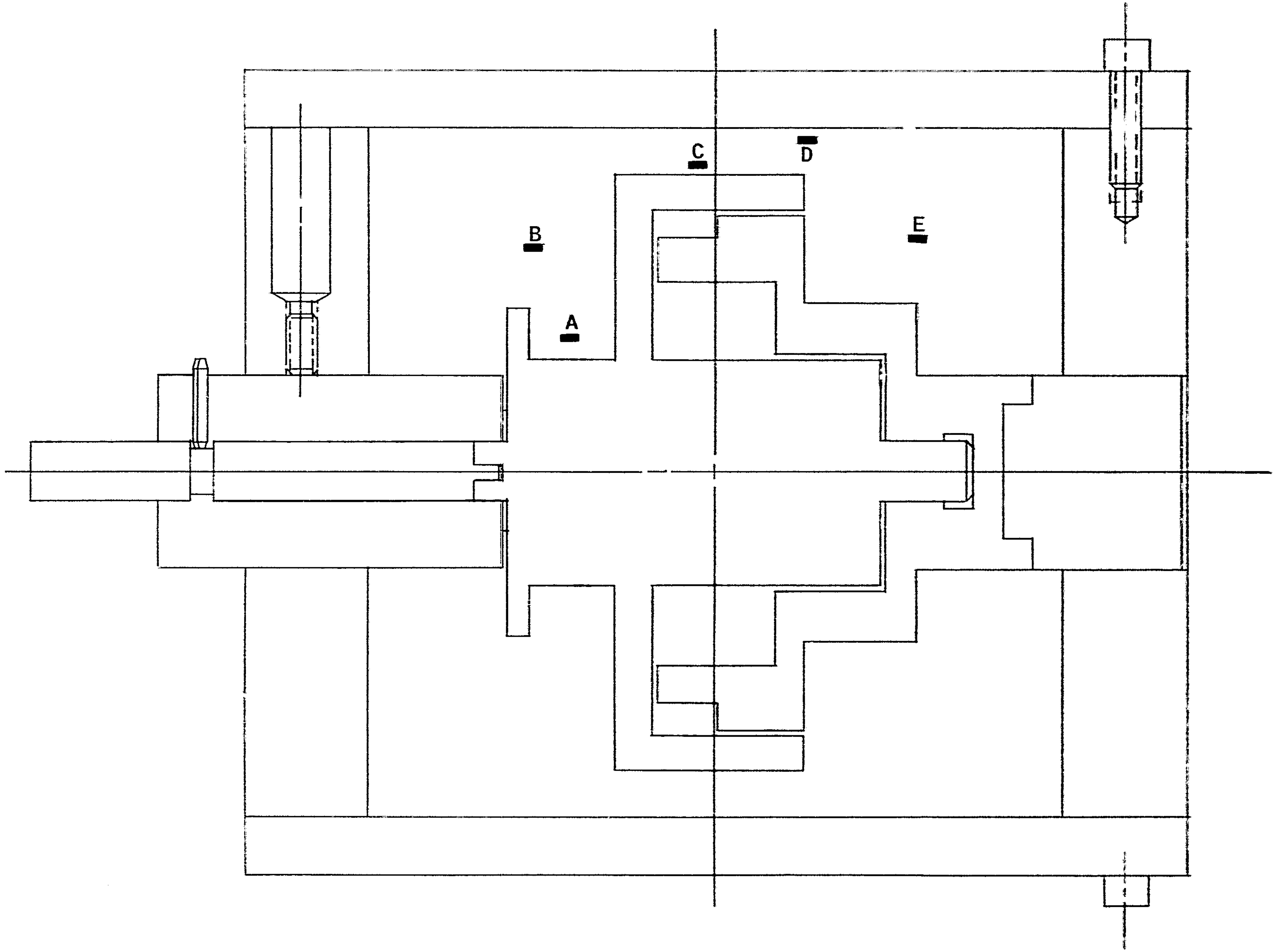

Figure 5. 4X Model and Probe Locations

the instrumented GG334 gimbal data serves to verify the accuracy of the scaling and provides a reliable baseline for evaluting the efforts to reduce tubulence.

Table II. Flow Characteristics of 4X Scale Model of GG334S Gimbal

Probe Location (Figure 5)	Velocity (ft/sec)	Δ Velocity (ft/sec)
A	1.38	0.9
B	0.75	0.6
C	5.00	0.6
D	0.62	0.9
E	0.25	0.15

Possible Methods of Reducing Windage Torques

Three direct methods of reducing the windage torques associated with the spinning rotor of the GG334S are to

- Reduce gimbal pressure to reduce the gas density and hence the angular momentum of the revolving gas
- Reduce operating speed of the rotor, thereby reducing the angular velocity and momentum of the gas which derives its speed from the motor
- Convert turbulent flow to smooth laminar flow by incorporating shrouds

For the GG334S gas-bearing spinmotor, a reduction in gimbal pressure would encompass a corresponding reduction in gas-bearing stiffness. Since the objective is to achieve approximately a 10:1 reduction in windage torques, shock capability, random vibration capability, and rate capability would be severely diminished as compared to their present levels if reduced pressure was used. A second undesirable effect of reduced pressure would be the possibility of introducing contaminants into the gimbal during assembly processes because of the partial vacuum condition that would exist. (Normal pressure in the gimbal is approximately 18 psia. This would have to be reduced to approximately 2 psia for noise reduction.)

A reduction in rotor speed offers no answer to noise reduction from a gyro standpoint because the ratio of angular momentum of the gas to that of the rotor would remain constant. Although windage would be reduced as measured in dyne-cm, it would remain constant when converted to deg/hr.

For these reasons the windage shrouds are considered to offer the most reasonable approach to reducing noise insofar as the amount of impact on other gyro parameters.

Shroud Design

The use of a shroud around the rotor reduces in two ways the error torques resulting from rotor windage currents. First, the total mass of spinning hydrogen is reduced. Secondly, the flow between the shroud and the rotor is stabilized so that a constant torque about the rotor axis is present instead of the random error torques which can result from an unsteady flow field.

The basic shroud is illustrated in Figure 6. The total volume of hydrogen in the gimbal is approximately 30 cc. The volume of hydrogen between the shroud and the rotor is approximately 3 cc. Hence, the mass of spinning hydrogen is reduced by an order of magnitude. Also, the radius of hydrogen gyration about the rotor axis is reduced by a factor of 1.8; hence, the total moment of inertia of hydrogen is reduced by a factor of 30. The angular momentum of the spinning hydrogen will be reduced by something less than a factor of 30, however, because the average angular velocity of the hydrogen between the shroud and the rotor will be approximately one-half the angular velocity of the rotor. Without the shroud, the irregular shape of the gimbal causes a completely separated flow field with significantly reduced angular velocity. Specifically, measurements in the separated flow field indicated flow velocities on the order of 5 to 16 ft/sec, which correspond to angular velocities at the locations measured on the order of one-tenth the angular velocity of the rotor. Hence, the net reduction in the angular momentum of the spinning hydrogen may only be a factor of 6. For this reason, the stability of the flow between the rotor and the shroud is important.

Basically, three types of unstable or unsteady flow can exist in the flow between a rotor and a shroud. The flow may be turbulent; Taylor vortices may develop on the cylindrical surfaces of the rotor; and secondary flow patterns may result from the boundary layer on the rotor faces (Figure 7).

The flow on the cylindrical faces of the rotor is best described by a Reynolds number which takes into account both the radius of the cylinder and the width of the gap between the rotor and the shroud. Specifically, the condition for the onset of Taylor vortex formation is

$$Rey_T = \frac{\rho v h}{\mu} \sqrt{\frac{h}{r}} > 41.3$$

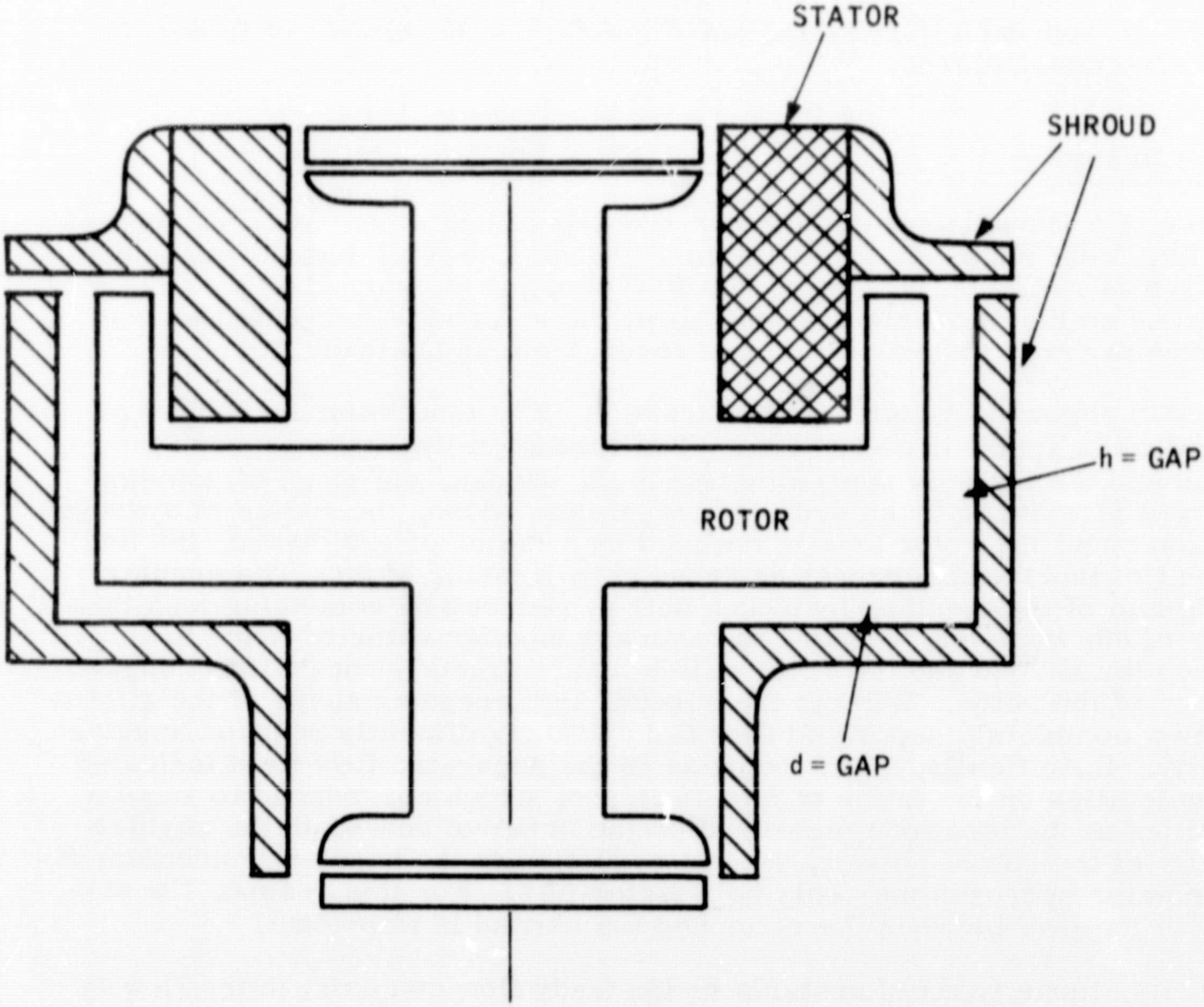

Figure 6. Rotor Shroud Configuration

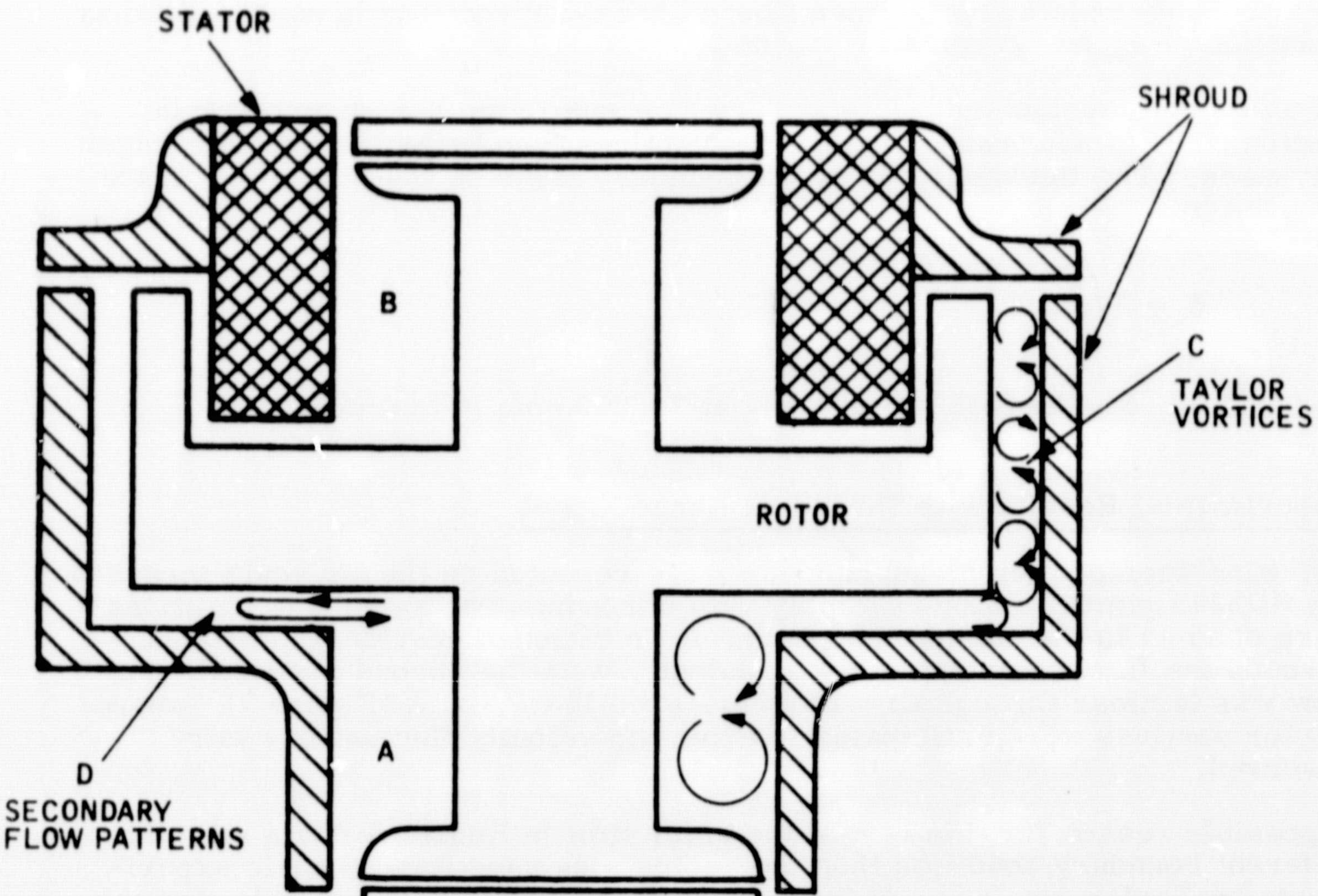

Figure 7. Possible Flow Instabilities Between Rotor and Shroud

where h is the gap between the shroud and the rotor. The flow in these vortices will remain laminar and stable up to a value of Rey_T = 1, 730.* To avoid the onset of Taylor vortices in Region C (Figure 7), the maximum allowable gap would be about 0. 022 in. In Regions A and B, the maximum allowable gap would be 0. 031 in. It is believed, however, that shrouding in Regions A and B would be difficult both from a construction and weight standpoint. For the shroud design indicated in Figure 7, the gap in Region A will be 0. 107 in. This will result in a Taylor Reynolds number of 270 and will probably result in a laminar flow with Taylor vortices present. Similar conditions may be expected in Region B.

To avoid the development of secondary flow due to the boundary layer in Region D, it is necessary to make the gap less than twice the boundary layer thickness. The thickness, δ, of the boundary layer on the face of the rotor is given by

$$\delta = \sqrt{\frac{\mu}{\rho\omega}}$$

or 0. 008 in. for the GG334S spinning at 24, 000 rpm in hydrogen.

Experimental Results with Shroud on Large Model

Hot-wire anemometer measurements were repeated on the 4X scale model of the GG334S gimbal motor assembly with shrouds. The same five locations were used as in the unshrouded tests. As mentioned previously, without shrouds the flow was completely turbulent. With the shroud installed, the flow was laminar throughout. Further, even in Region A (Figure 7), where Taylor vortices were anticipated to exist, no velocity fluctuations were observed.

A possible reason for this is that the rotor flow in Region A has a slightly different boundary condition than the geometries used for the basic experiments on Taylor vortices. If these results are valid, it is possible that the shroud will reduce fluctuating components in the windage torque to zero. Figure 8 and Table III present the results of the flow measurements for the shrouded model.

Visual Tests

To provide conclusive checks on the results of the anemometer measurements, flow visualization tests were also conducted on the 4X scale model. These

*Schlichting, H.: Boundary Layer Theory. McGraw Hill, 1955.

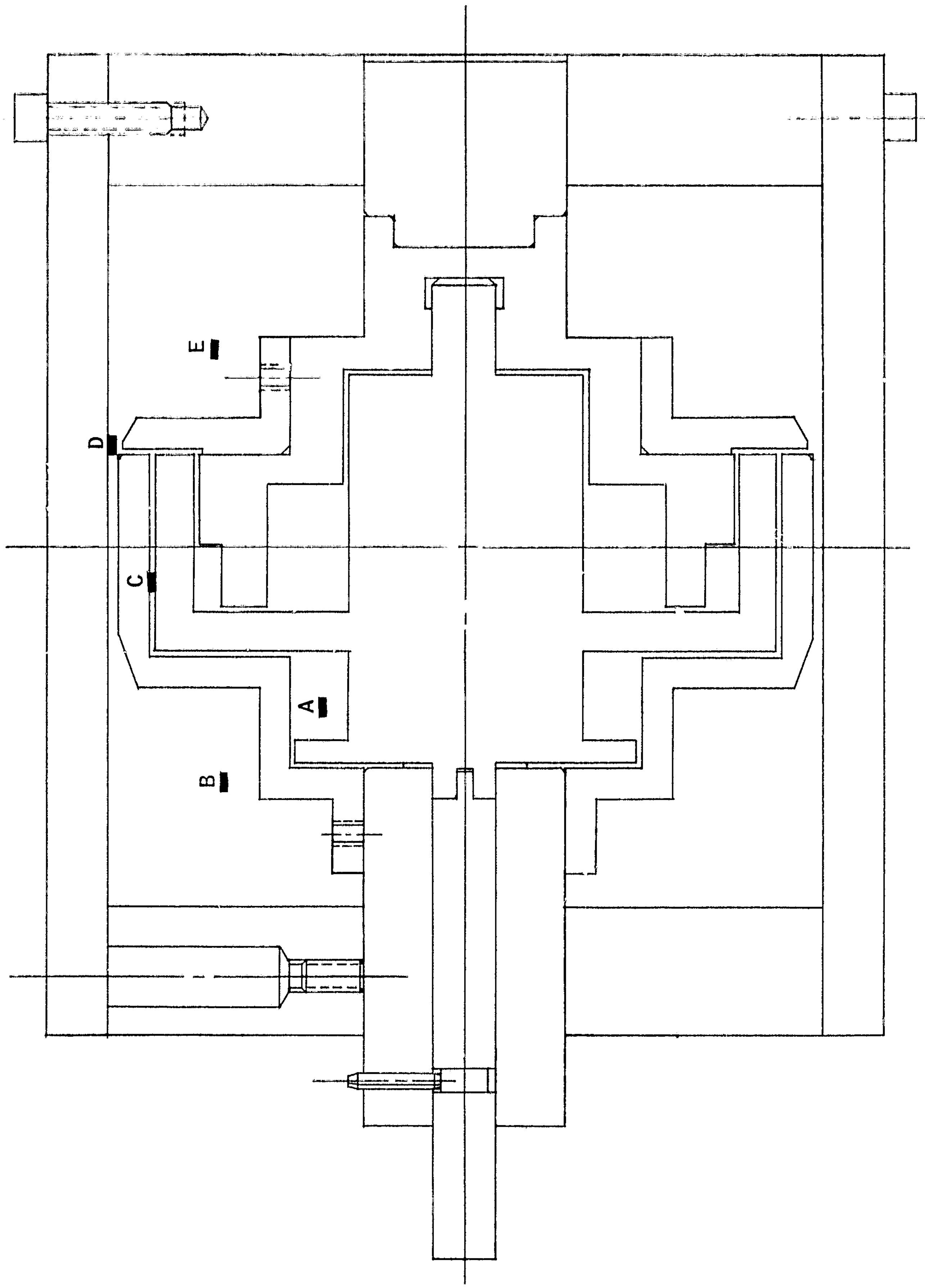

Figure 8. 4X Model with Shrouds

Table III. Flow Characteristics of 4X Scale Model with Shrouds

Probe Location (Figure 7)	Velocity (ft/sec)	Δ Velocity (ft/sec)
A	2.5	0*
B	0	0
C	3.7	0.06**
D	0	0
E	0	0

*Readout limitation, 0.03 fps

**Periodic fluctuation resulting from runout in rotor

tests were conducted using dye filaments with the model operating in water. The rotor speed for these tests was reduced to 0.4 rps, which provided a Reynolds number of 5600. Figure 9 shows the turbulence present around the periphery of the momentum ring in the unshrouded case. Figure 10 shows the same region with the shroud installed. As can be seen, a steady laminar flow was obtained.

Figure 11 shows the result of dye filament introduced in the region between the rotor's momentum ring and thrust surface with no shrouds present. As in Figure 9, the flow is disoriented and turbulent. Figure 12 shows the dye filament in the same region with the shrouds. In all cases with the shroud, a steady laminar flow was obtained. These results are consistent with the earlier measurements in an air environment using the hot-wire anemometer.

One conclusion reached during this visualization study was that the flow in the region shown in Figure 12 is only marginally stable. A slight increase in rotor speed (i.e., 0.4 to 0.5 rps) resulted in a secondary flow as seen by breakup of the dye filament. The region shown in Figure 10 is stable over a large increase in rotor speed, showing no breakup in the dye filament up to 1 rps.

Secondly, it was seen that an axial pumping took place between the rotor and shroud if the shroud was vented on both ends. Sealing either one of the vented regions eliminated this effect. This pumping action would tend to disrupt the stability of the flow shown in Figure 12.

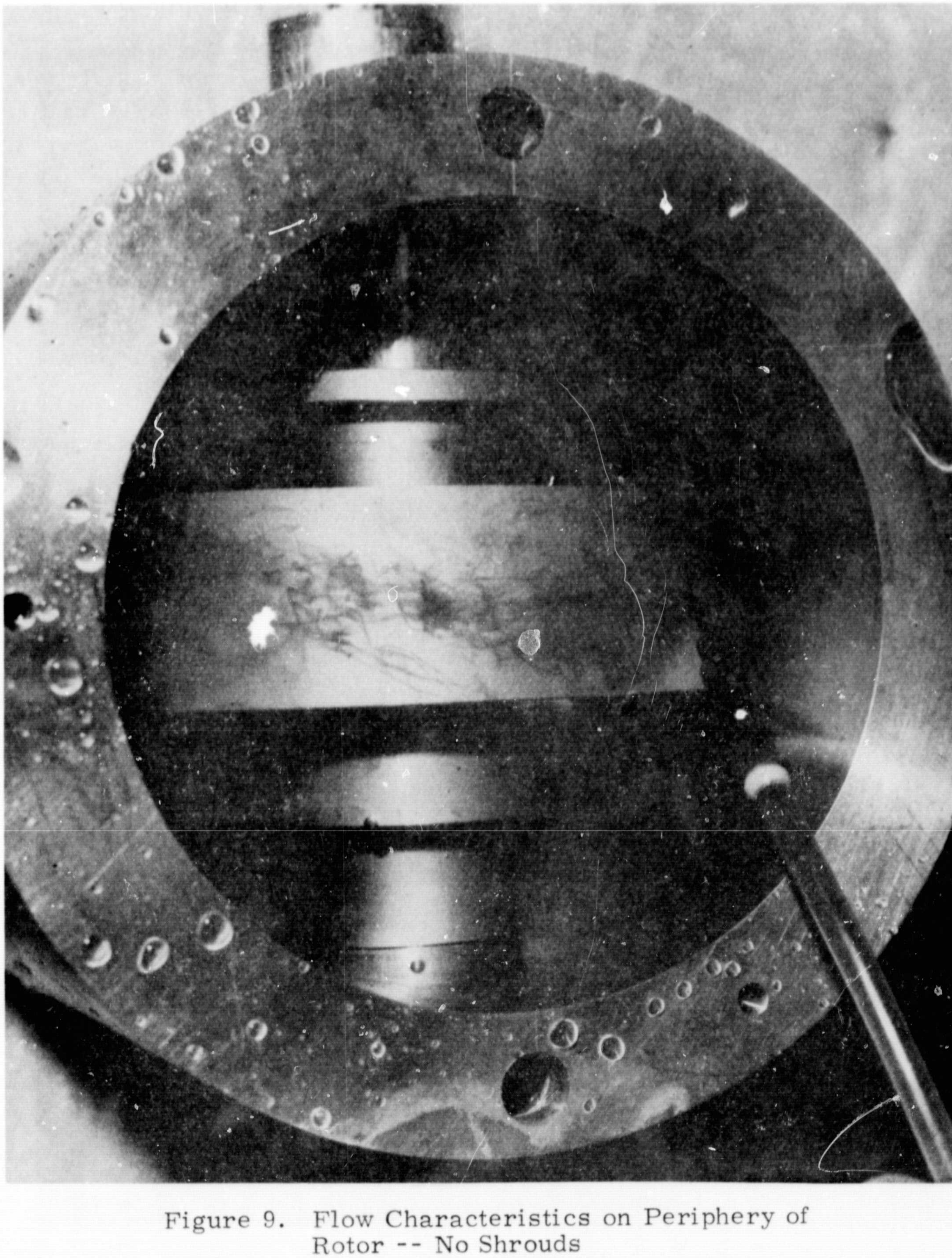

Figure 9. Flow Characteristics on Periphery of Rotor -- No Shrouds

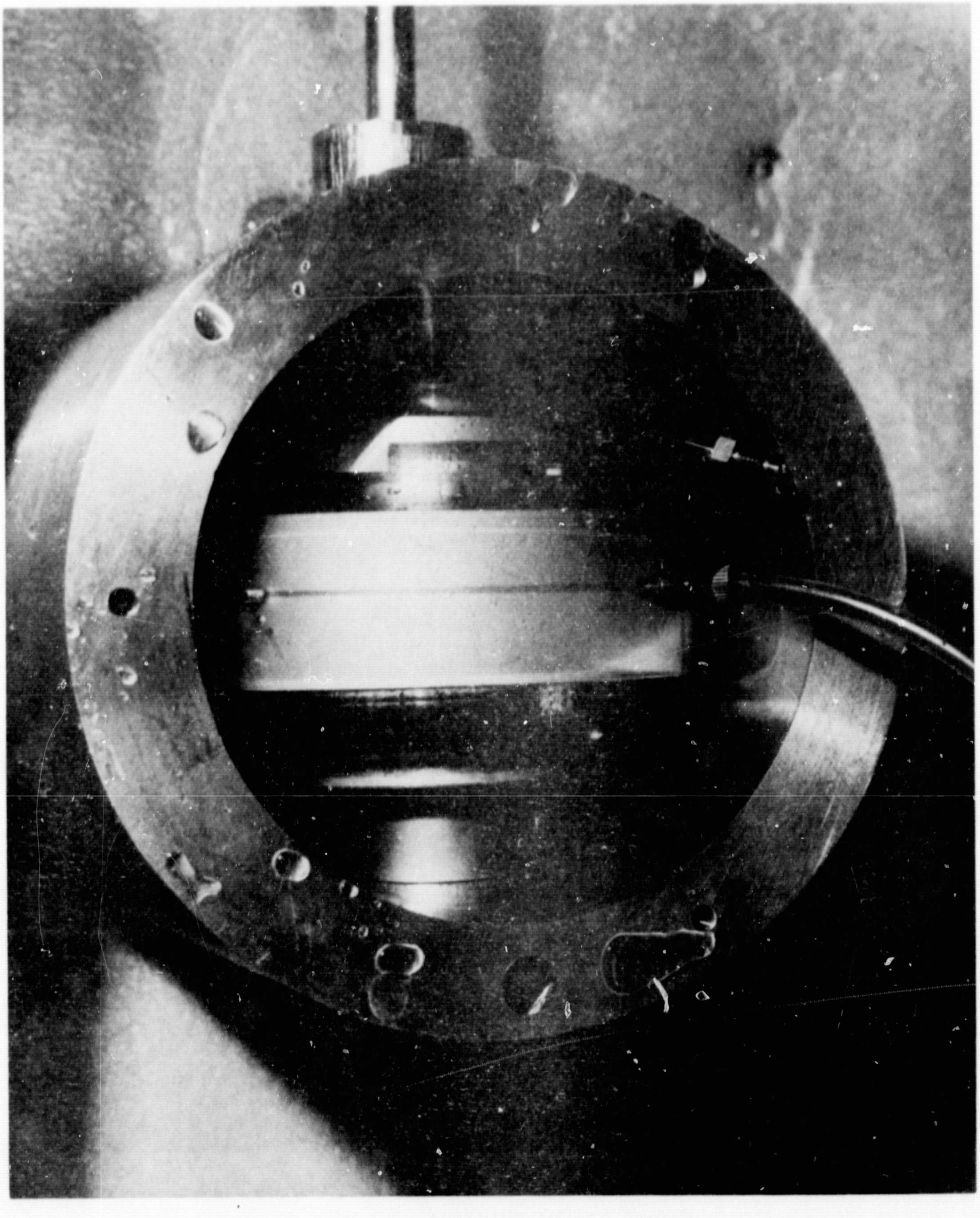

Figure 10. Flow Characteristics on Periphery of Rotor -- With Shrouds

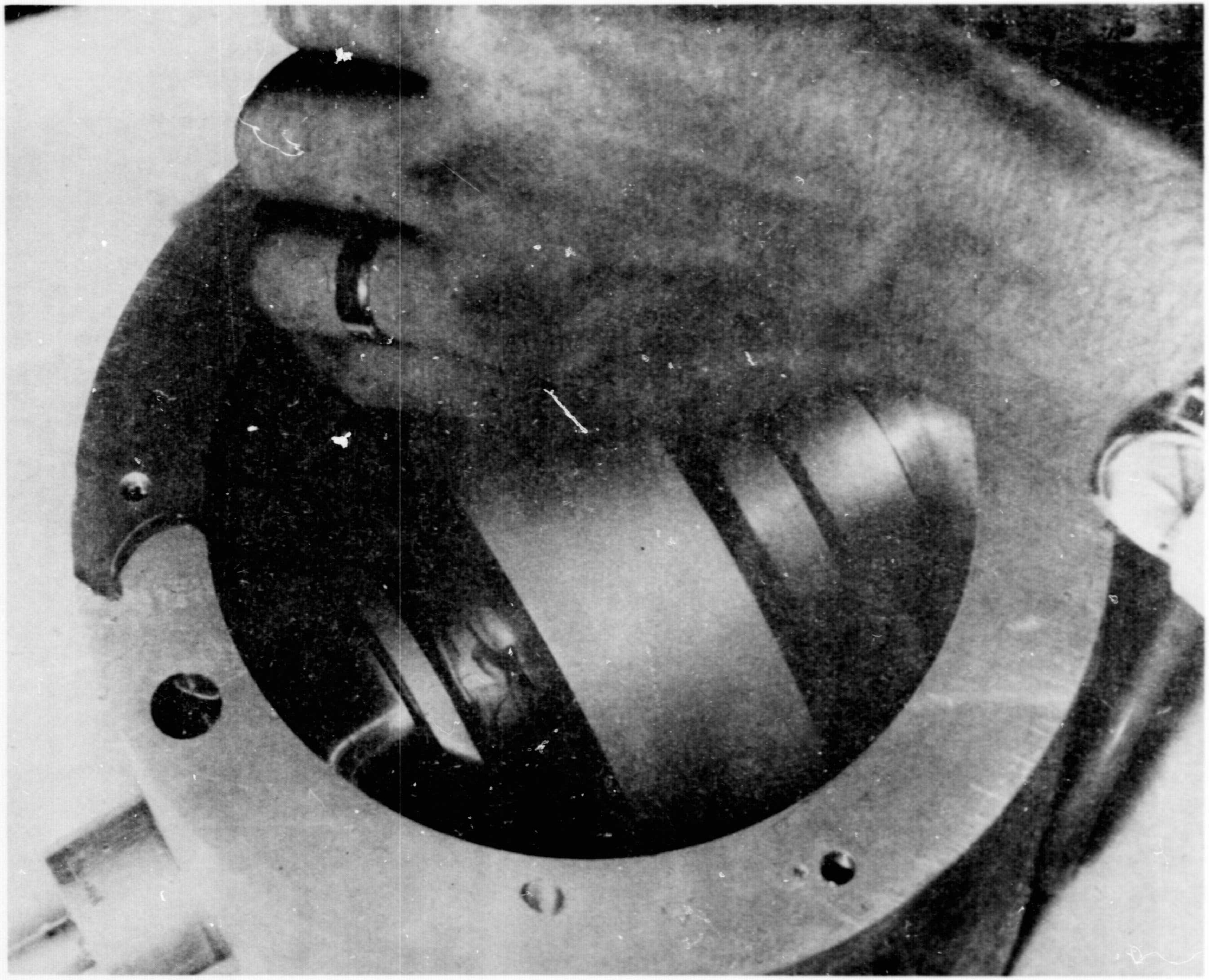

Figure 11. Flow Characteristics in Rotor Thrust Cavity -- No Shrouds

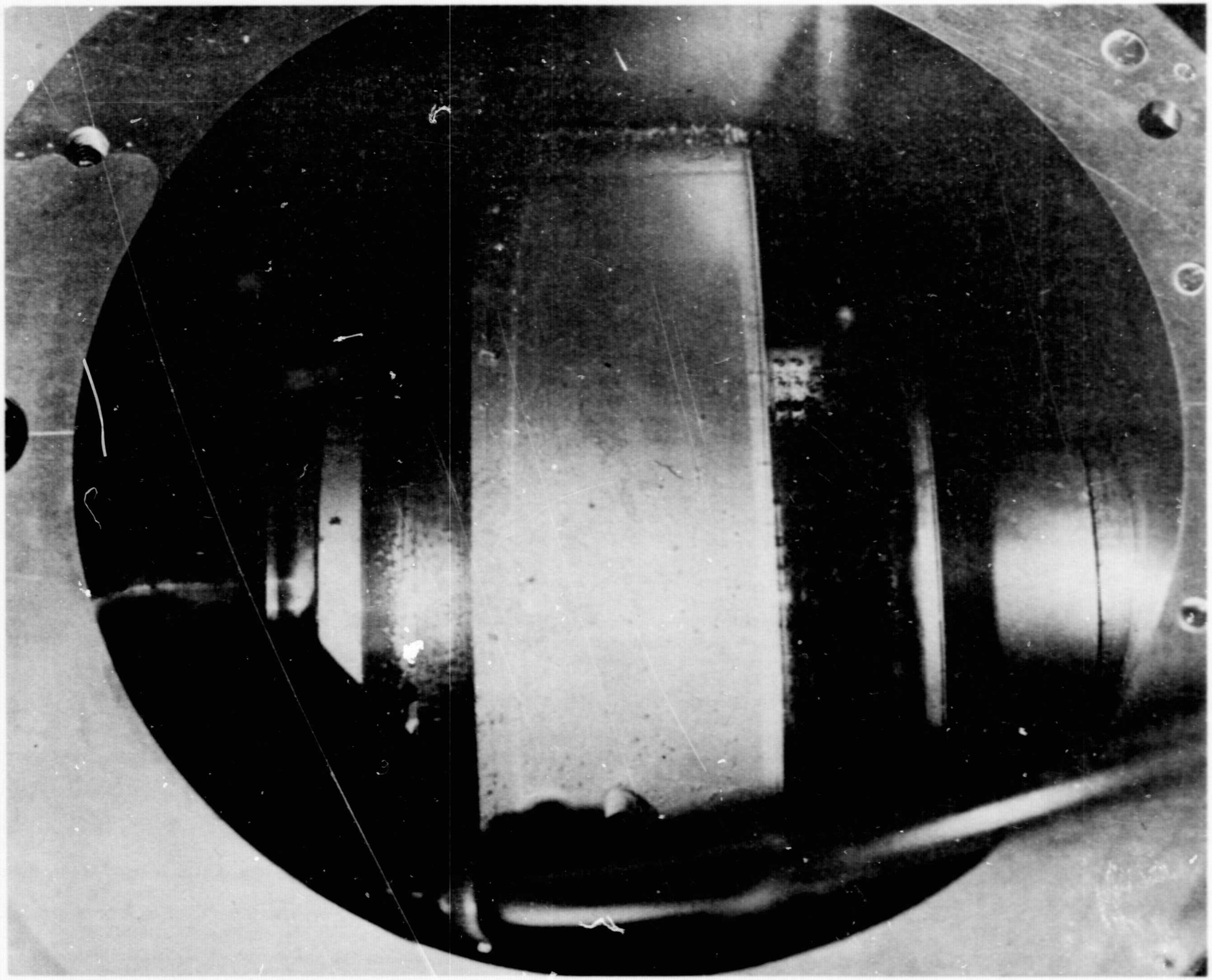

Figure 12. Flow Characteristics in Rotor Thrust Cavity -- With Shrouds

The flow visualization shown in Figure 10 was repeated to determine the effect of "V" grooves and balance holes in the face of the rotor. Two "V" grooves 0.016 in. deep and 24 randomly located balance holes 0.128 in. in diameter were placed in the rotor. The flow characteristics shown in Figure 10 were unchanged except when the dye filament was introduced directly over the "V" grooves. In this case, a slight widening of the filament was observed over the grooves, but there was no indication of turbulence.

DESIGN AND TEST OF IMPROVED SUBASSEMBLY HARDWARE

Shroud Design and Fabrication

Windage shrouds were designed and fabricated for the GG334S motor based on the guidelines established during the test of the 4X model. Figure 13 is a layout drawing of the shrouds shown in conjunction with the motor and gimbal ID. Separation between the shroud and motor is held to 0.010 in. nominal, as suggested by the studies on the 4X model where the separation was 0.040 in. The larger shroud section is held to the zircalloy shaft by means of threads and thereby replaces the holding nut previously used. The smaller shroud is held to the larger by the means of four screws located in appendages of both shroud sections (Figure 14). The two shroud sections are joined at the edge of the rotor's momentum ring to prevent any discontinuity in the shroud in this high-velocity region. The smaller shroud is mounted also to the existing beryllium stator hub and held in place by a fillet of epoxy.

Weight -- For the design shown with a wall thickness of 0.030 in. and constructed of beryllium (density = 1.85 g/cc), the shroud would weigh approximately 4.5 gm. Since the shrouds are not a structural member meant to support appreciable loads, they could theoretically be made thin without affecting their function. For beryllium, however, 0.030 in. appears to be a good workable dimension since it can be machined directly without resorting to expensive lapping techniques to obtain thickness on the order of 0.020 in. The weight of the shrouds increases the motor assembly weight by about 10 percent and as such is not prohibitive from an overall gyro design consideration.

Load Torque Resulting From Viscous Drag on the Rotor -- With a closely spaced shroud, the velocity distribution in the flow between the shroud and the rotor will vary linearly from 0 at the shroud to the local surface speed of the rotor. The viscous shear stress is then

$$\tau = \mu \frac{V}{h}$$

The total torque on the rotor in the GG334S with the gaps h and d both equal to 0.010 in. will be 256 dyne-cm. If the gap h is increased to 0.020 in., the total torque will be reduced to 161 dyne-cm. Since this is approximately the

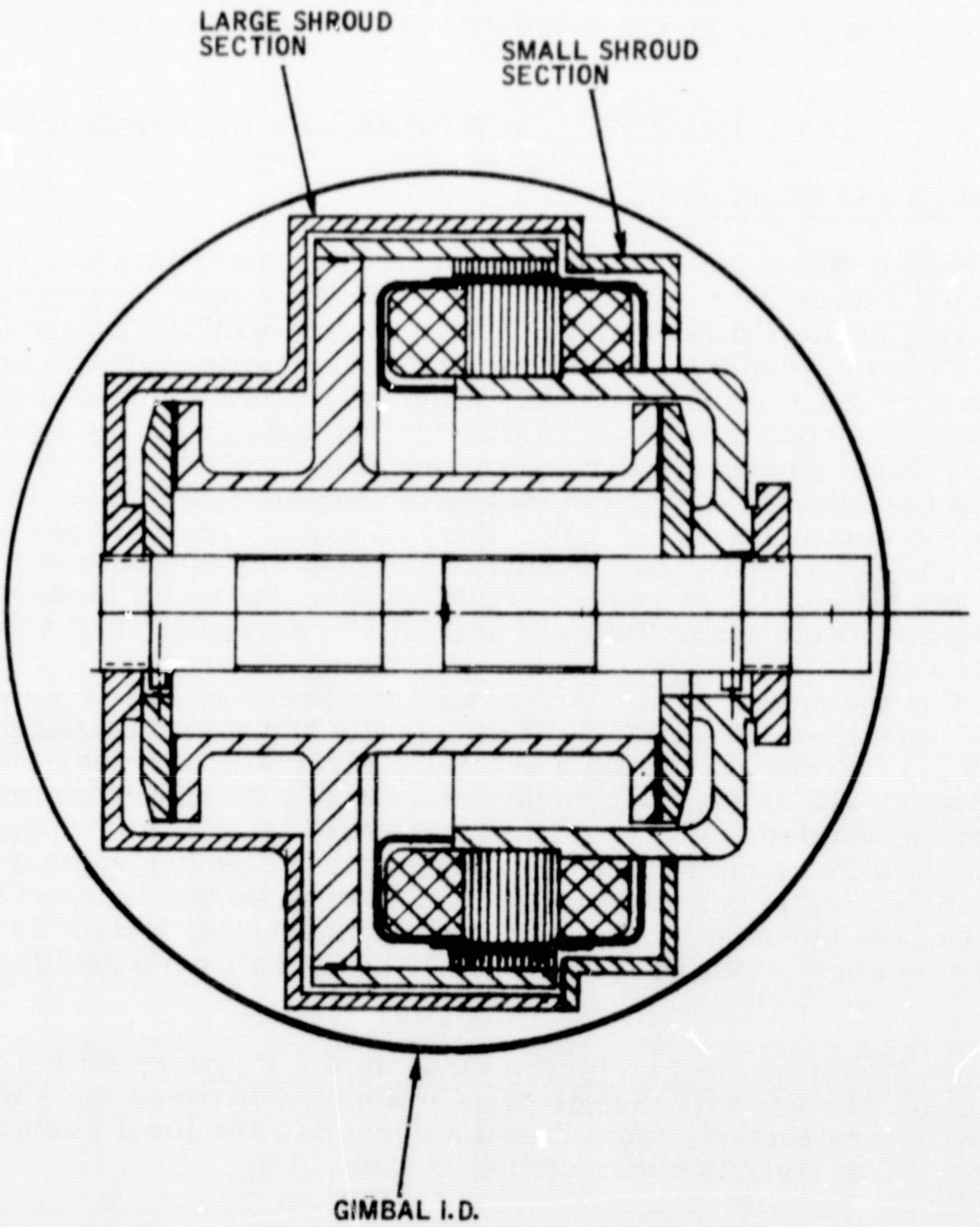

Figure 13. Layout Drawing - Shroud and Motor View Along Gyro O. A.

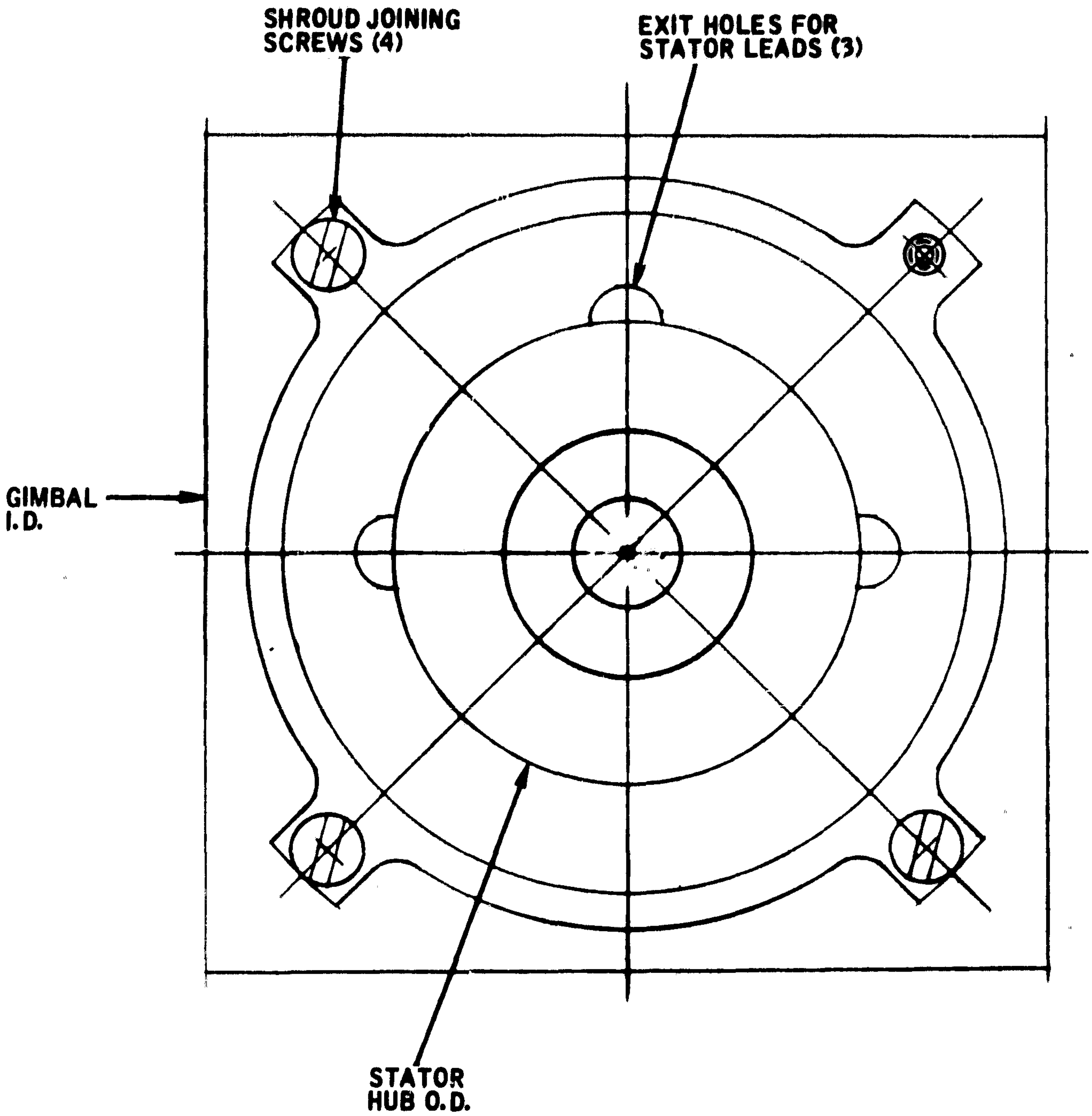

Figure 14. Shroud Layout - View Along S. A. from Stator End

same magnitude of windage torques with which we originally started, there is no net increase in load torque on the motor and hence no power increase. In essence, turbulent windage torques were traded for laminar drag torques.

Contribution of Shrouds to Anisoelastic Coefficient -- An estimate of the contribution of the spinmotor shroud on the GG334S g^2 coefficient was made by assuming that the shroud was a lumped parameter spring-mass system. Since the shroud is, by sight, stiffer radially than axially, worst-case anisoelastic coefficient was calculated by assuming no radial deflection.

This approximate analysis shows that the g^2 torque caused by the shroud will be 2.1×10^{-4} dyne-cm/g^2 for steady accelerations. For the GG334S angular momentum, this amounts to 0.0004 deg/hr/g^2, or two orders of magnitude less than the present device capability. For this reason, a more refined analysis is not required.

The anisoelastic torque analysis also showed that the structural resonance of the shroud system will be approximately 15 KHz, well above the typical 2-KHz vibration inputs.

Mass Stability of Shrouds -- To determine potential g-sensitive torque instability associated with the windage shrouds, an analysis was conducted to determine the stress levels in the beryllium members that could be incurred by the environments of shock, random vibration, and temperature excursions. The following is a tabulation of maximum stress in the beryllium shroud versus environment.

Environment	Maximum Stress (psi)
200 g, 0.7 ms shock	1300
25 g rms random vibration	490
±100°F temperature excursion*	5700

*Assumes zero stress at cure temperature of epoxy, typically 180°F to 220°F.

For the environments described, the stress levels are well below the published micro yield stress of 9000 psi for beryllium. The largest stress occurs during temperature excursions, and this is caused by the thermal mismatch between the zirconium shaft of the GG334S (3.1×10^{-6} in./in./°F) and the beryllium shroud which is joined to the shaft (6.4×10^{-6} in./in./°F).

A cooldown to 0°F, based on a zero stress point of 180°F, would produce 10,300 psi stress in the beryllium shroud and perhaps generate mass shifts.

This mechanism could be reduced or even eliminated by a different choice of shaft material (i.e., the beryllium shafts used on other GG334 devices).

<u>Effects of a Windage Shroud on Gas-Bearing Performance</u> -- A windage shroud which changes turbulent flow to laminar flow at the gas-bearing boundaries (exit and entrance regions) is not expected to influence gas-bearing performance.

Gas-bearing performance is dependent on the ratio of viscous gas forces to pressure forces summed over an appropriate area of the bearing. A dimensionless number commonly used to describe gas-bearing performance is the Compressibility Number

$$\Delta = C \frac{\omega\mu}{p} \left(\frac{r}{h}\right)^2$$

where

Δ = Compressibility Number

C = dimensionless constant

ω = angular speed (rad/sec)

μ = gas viscosity (lb sec/in^2)

p = ambient pressure (lb/in^2)

r = bearing radius (in.)

h = bearing clearance (in.)

As long as this Compressibility Number remains unchanged at the boundaries of the bearing, no change in gas-bearing performance will occur.

The parameters of angular speed, radius, and clearance at boundaries (e.g., a thrust plate outside diameter) remain unchanged with or without a shroud. The parameters of gas viscosity and ambient pressure should not change as the nearby gas is turbulent or laminar. Therefore, a windage shroud which changes turbulent flow to laminar flow at the boundaries of a gas bearing is not expected to influence performance.

Subassembly Tests

The spinmotor from GG334S S/N B-3 was assembled and tested to obtain motor performance data both with and without windage shrouds. Key spinmotor parameters were measured at the spinmotor level before and after installation of shrouds and also at the final gimbal assembly level. These data are summarized in Table IV. As can be seen from the data, motor performance remained constant, within measuring capability, through the various conditions. This is in agreement with previous analysis, indicating no increase in load torques due to the addition of shrouds.

A floated, temperature-controlled dynamometer was modified to accommodate the GG334S gimbal in a neutrally buoyant mode. Figure 15 shows the dynamometer with the GG334S gimbal attached. Figure 16 diagrams the dynamometer setup.

A 25-Hz, first-order loop was established by caging the dynamometer through its precision torquer. Noise data were then obtained on a peak-to-peak basis via oscilloscope and on an rms basis with an rms-voltmeter for both the motor-on and motor-off conditions. The loop was maintained at a 25-Hz bandwidth with noise measured over various frequency ranges from 4 Hz to 25 Hz by using a fifth-order Allison filter. The entire test setup is diagrammed in Figure 17. Table V summarizes the test results.

The noise over 25 Hz increased approximately 20% motor-off to motor-on, where previous noise data at the gyro level showed increases of greater than 700%.

To obtain comparative dynamometer noise data on a gimbal assembly with an unshrouded motor, the dynamometer was rebuilt with a GG334A1 gimbal assembly. The motor-gimbal configuration of this unit is very similar to that of the GG334S. In addition, gimbal weights and inertias were within 10%, allowing the test to be conducted with the same loop parameters. Angular momentum of the GG334A motor, however, is twice that of the GG334S, which produces a factor of 2 reduction in noise in deg/hr for identical noise on a torque basis. Table VI summarizes the test results on this unit. Taking into account the increased angular momentum, the motor-off noise agrees extremely well with the motor-off noise on the GG334S gimbal assembly, which is indicative of the repeatability of the dynamometer test fixture through reassembly. Motor-on noise for this unshrouded motor shows the typical large increase noted in previous tests and is greatest in the 0- to 25-Hz case (600%).

In addition to the peak-to-peak and rms measurements, PSD measurements were made on both the shrouded and unshrouded vehicles for motor-off and motor-on conditions. Figure 18 shows the PSD curve for the unshrouded GG334A motor and Figure 19 shows the PSD curve for the GG334S shrouded

Table IV. Motor Performance With and Without Shrouds

Parameter	Motor Level, No Shrouds	Motor Level, With Shrouds	Gimbal Level With Shrouds
Starting Voltage (v)			
SA Horizontal	16	16	16
SA Vertical Up	16	17	15.5
SA Vertical Down	16	18	16
Runup Time (sec)	9.6	10	9.2
Rundown Time (sec)	65	63.5	63.2
Minimum Synchronous Voltage	17	17	17
Power (w)			
Start	9.4	9.1	9.8
Run	5.2	5.15	5.5

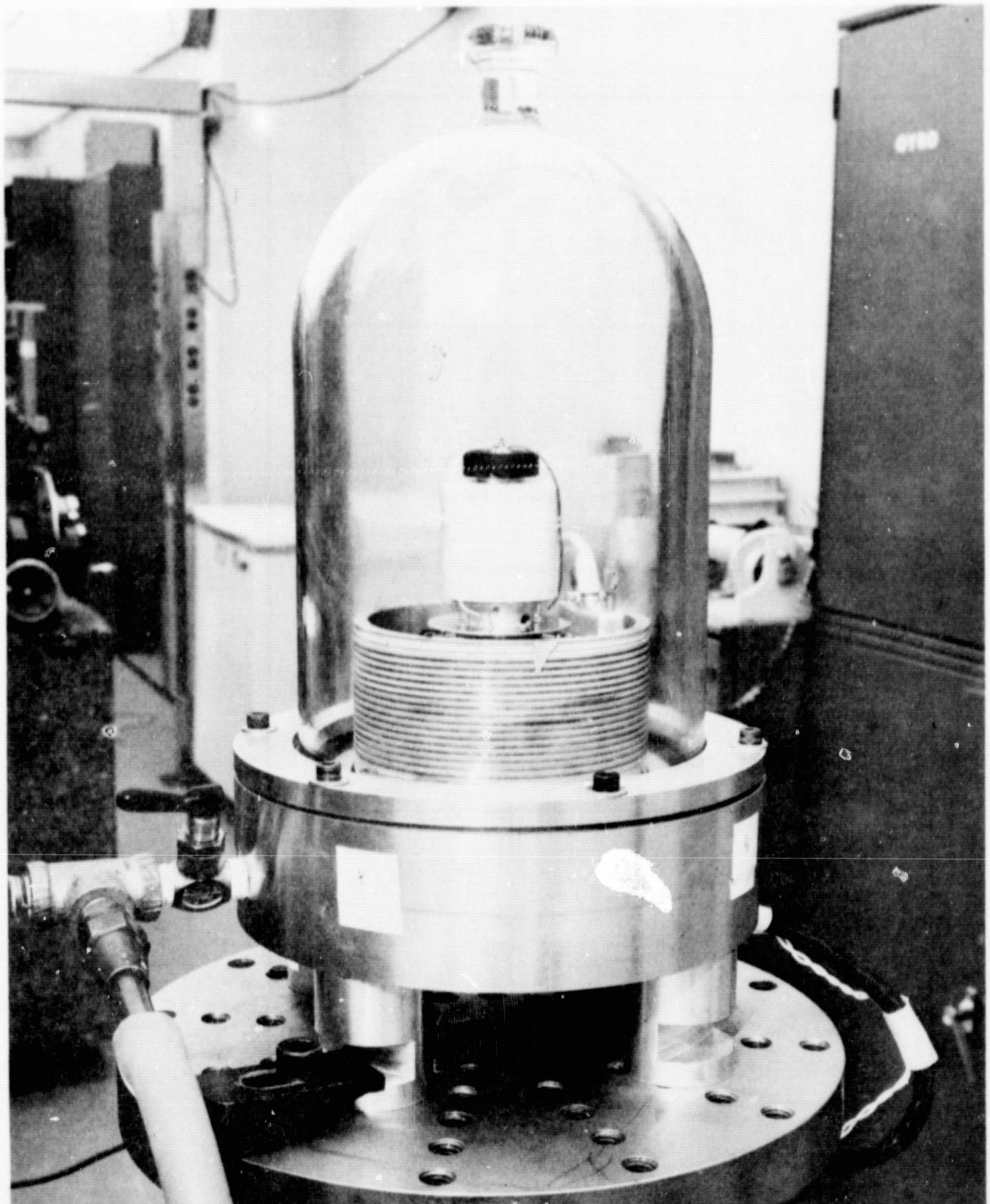

Figure 15. Dynamometer with GG334S Gimbal

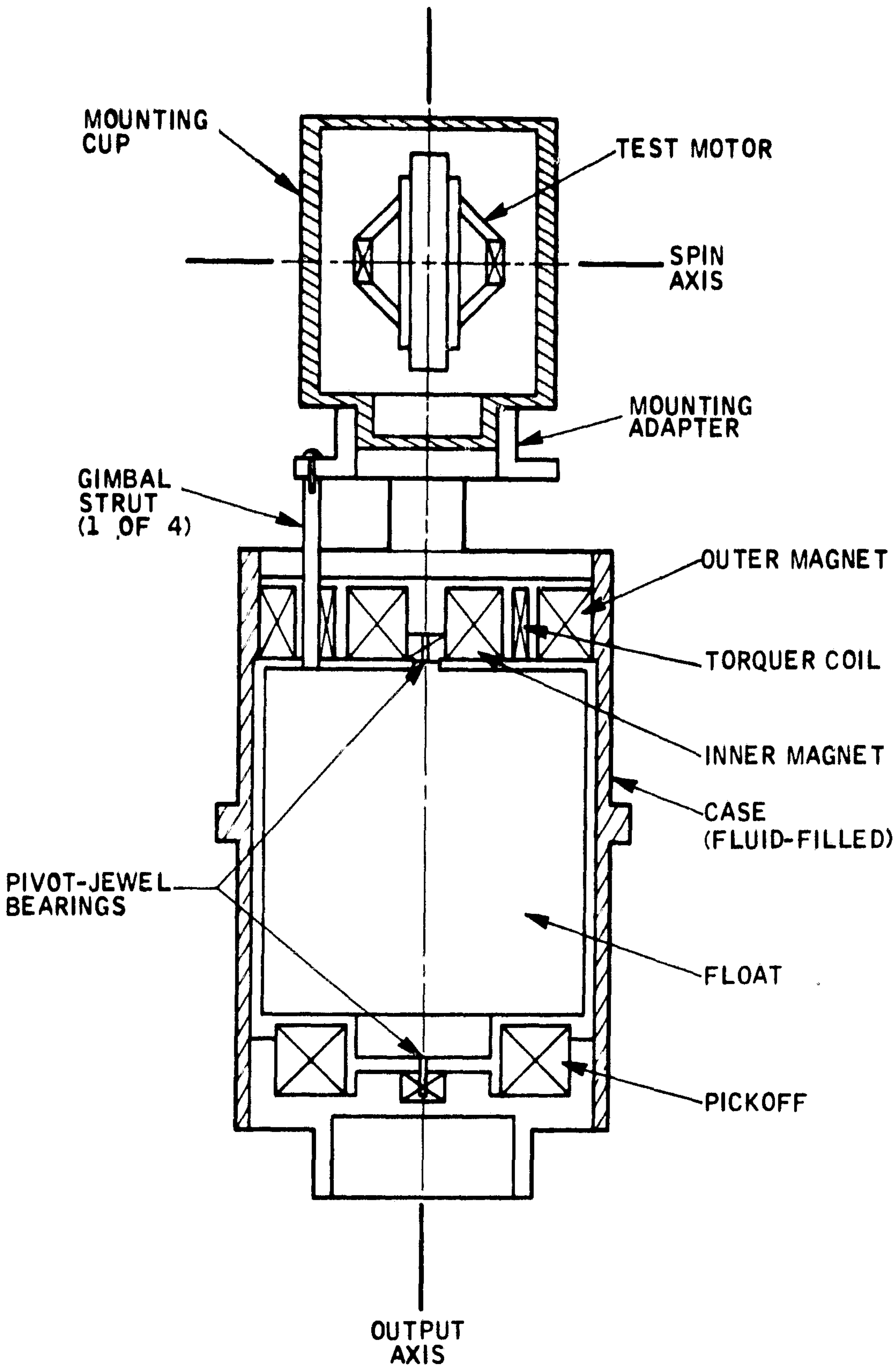

Figure 16. Dynamometer Test Fixture

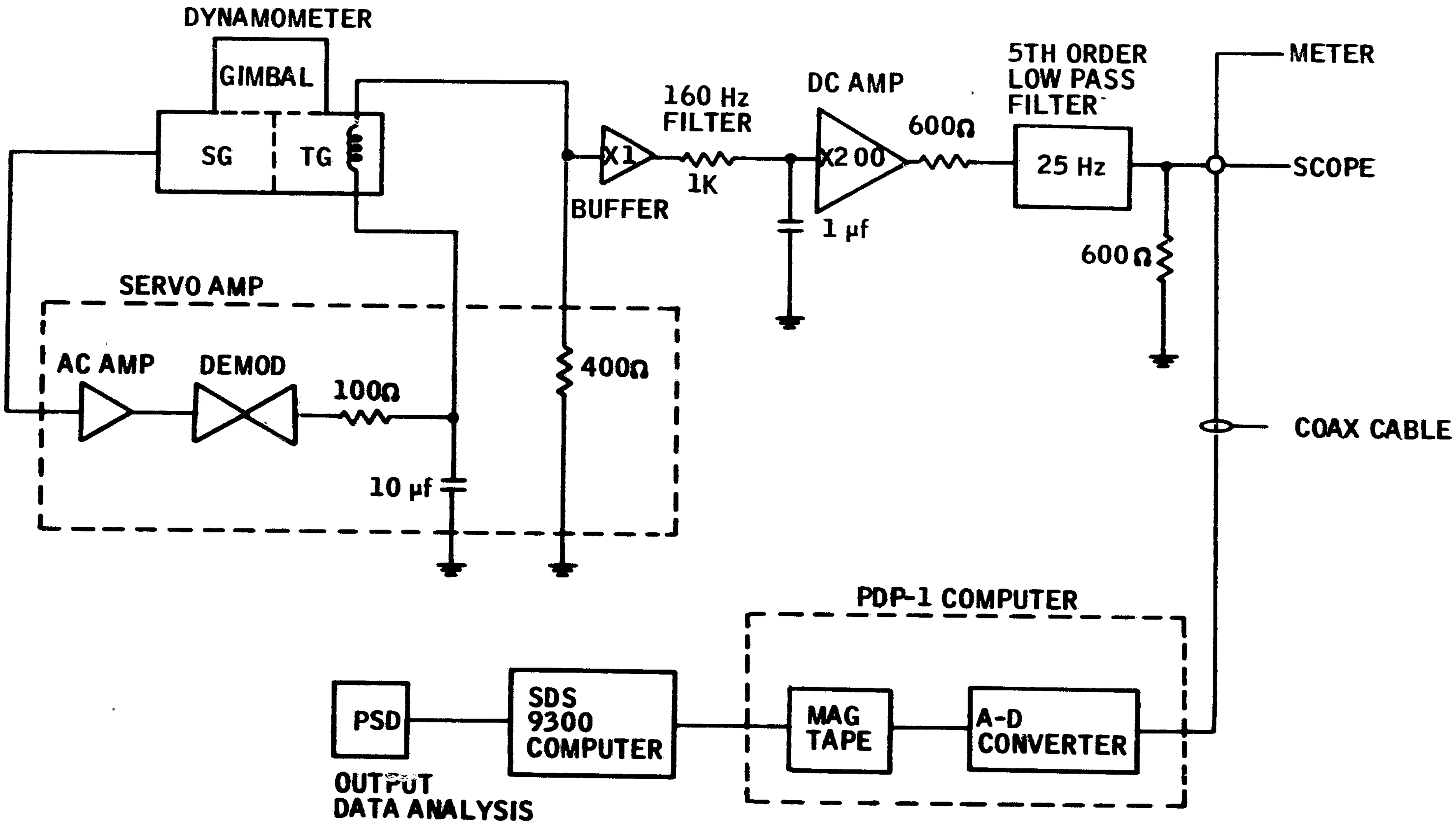

Figure 17. Noise Analysis Block Diagram

Table V. Noise Test Results on Shrouded GG334S Motor in 25 Hz Loop

Measurement Bandwidth (Hz)	Peak-to-Peak Noise (deg/hr)		RMS Noise (deg/hr)	
	Motor Off	Motor On	Motor Off	Motor On
0 to 25	1.60	2.00	0.34	0.46
0 to 15	0.70	0.80	0.20	0.20
0 to 10	0.60	0.60	0.15	0.15
0 to 4	0.20	0.40	0.08	0.07

Table VI. Noise Test Results on Unshrouded GG334A1 Motor in 25 Hz Loop

Measurement Bandwidth (Hz)	Peak-to-Peak Noise (deg/hr)		RMS Noise (deg/hr)	
	Motor Off	Motor On	Motor Off	Motor On
0 to 25	1.00	6.00	0.25	1.30
0 to 15	0.75	2.50	0.18	0.80
0 to 10	0.50	1.50	0.15	0.46
0 to 4	0.30	0.75	0.10	0.18

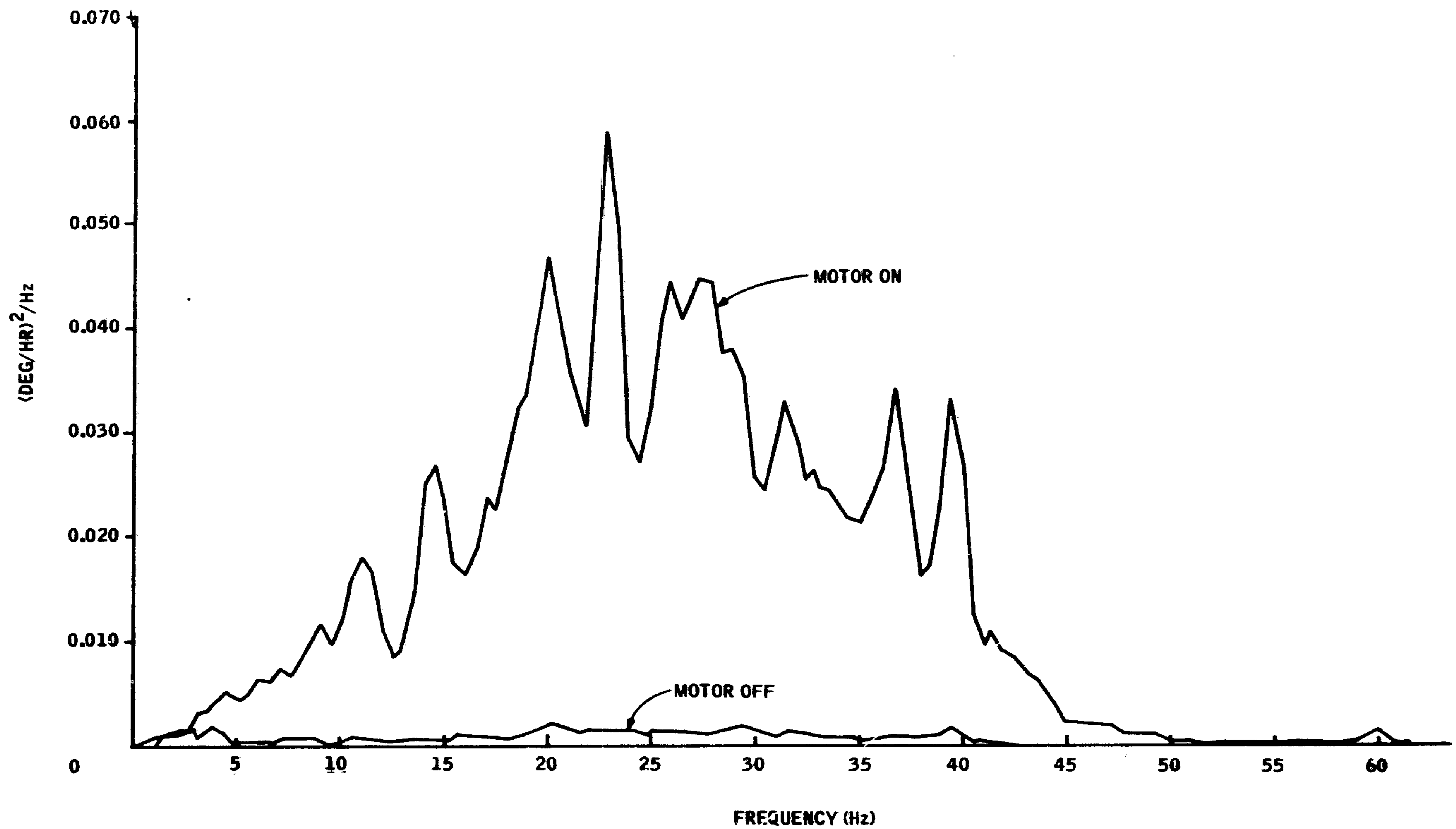

Figure 18. GG334A1 Gimbal Non-Shrouded Motor Power Spectral Density - 25 Hz Loop

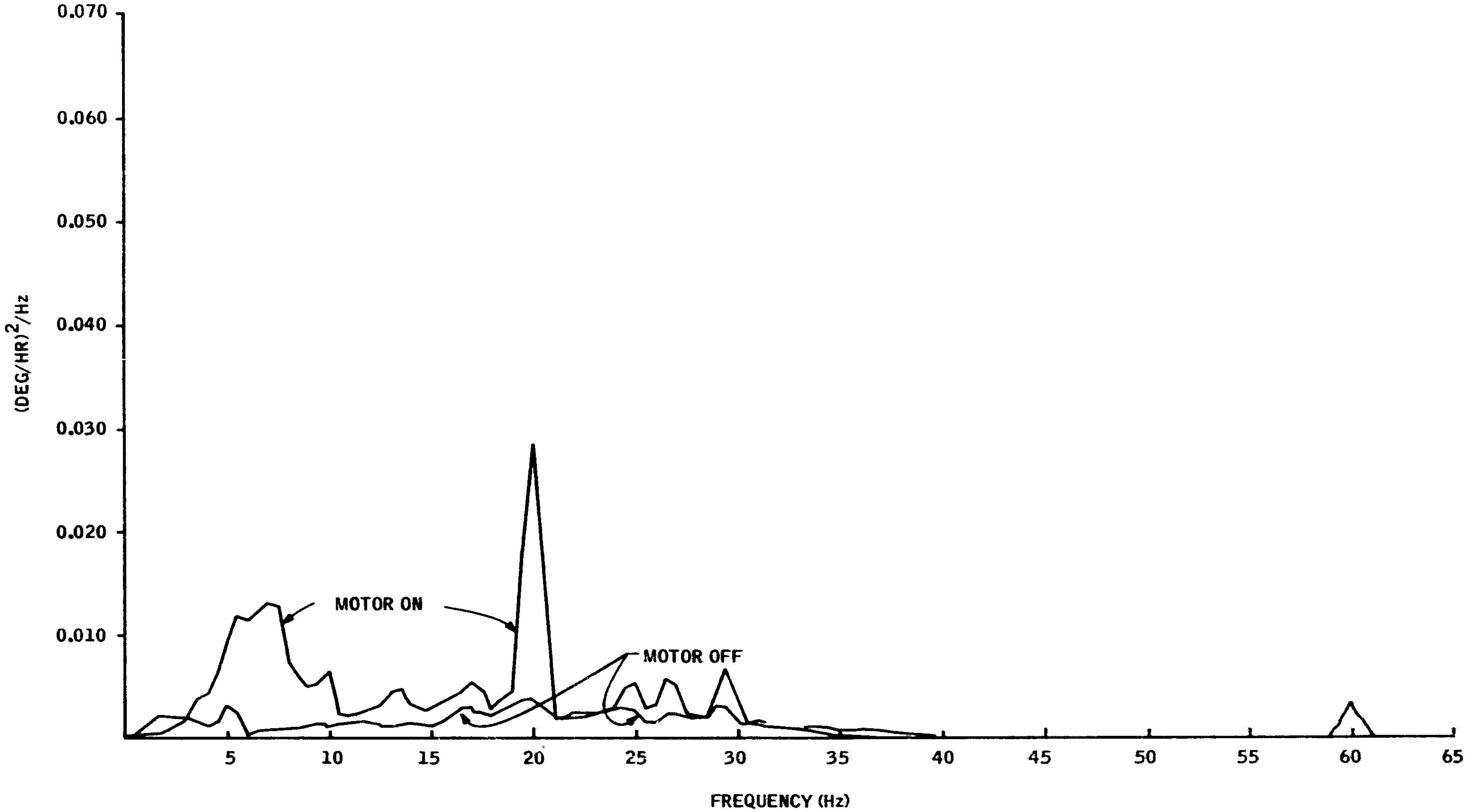

Figure 19. GG334S Gimbal W/Motor Shrouds Power Spectral Density - 25 Hz Loop

motor. In both cases, the loop was 25 Hz with the Allison filter set at a bandpass of 0 to 25.6 Hz. In Figure 19 the two predominant frequencies at approximately 6 and 20 Hz are due to test stand disturbances being picked up as rate motion by the gyro. The 20-Hz spike has appeared on virtually every noise test conducted at this facility and has been speculated to be the effect of the air conditioning units on the building. This frequency has been verified by seismometer tests. The 6-Hz component appears to be related to activity within the factory, such as various machines and pumps. This component appears to be greatest in amplitude during working hours and diminshes in the after hours periods. In the unshrouded motor tests these seismic disturbances are of negligible importance due to the magnitude of the windage torques. It now appears that after eliminating windage noise, seismic disturbances will have to be reexamined as to their effects on gyro noise in any future work. It is reasonable to assume that the 20% increase in noise, motor-off to motor-on (Table V), is due primarily to test stand motion seeen as rate inputs by the excited gyro.

These test data indicate that turbulent windage torques were virtually eliminated by incorporating the shrouds on the GG334S motor assembly. Also, the elimination of this turbulence has resulted in a noise reduction over the 25-Hz loop bandwidth by an approximate factor of six, based on the GG334A unshrouded test data.

The absolute value of peak-to-peak noise based on the dynamometer tests is 1.60 deg/hr (assuming that the 20% increase over this amount is due to test stand motion). Since this is above the required level of 1.0 deg/hr, an increase in angular momentum of the GG334S appears to be a practicable method of attaining the additional noise reduction.

An increase from 1.0×10^5 to 2.0×10^5 gm-cm/sec^2 would provide a gyro with noise characteristics of 0.8 to 1.0 deg/hr peak-to-peak over 25 Hz, thus meeting the noise requirements and still maintaining compatibility with other basic GG334S design characteristics.

Gyro Testing

An engineering GG334A gyro was modified with windage shrouds in order to obtain noise data at the gyro level and verify that elimination of turbulence in conjunction with an increase in wheel angular momentum would provide the required 1.0 deg/hr peak-to-peak noise. This test vehicle was chosen because (1) its similarity to the GG334S allowed use of the same basic shroud design, (2) the angular momentum of this gyro was twice that of the GG334S, and (3) a sufficient data base existed for comparison purposes (Section II).

Gyro noise testing was accomplished using the same instrumentation depicted in Figure 17 for the dynamometer testing. As before, a 25-Hz, first-order loop was established by capturing the gyro through its precision torquer.

Noise data were then obtained on a peak-to-peak and rms basis for both the motor-on and motor-off conditions. The loop was maintained at 25 Hz and noise was measured over various bandwidths from 4 Hz to 25 Hz by using a fifth-order filter. These data are presented in Table VII.

Table VII. Gyro Noise Test Results on Engineering GG334A Gyro in 25 Hz Loop

Measurement Bandwidth (Hz)	Peak-to-Peak Noise (deg/hr)		RMS Noise (deg/hr)	
	Motor Off	Motor On	Motor Off	Motor On
0 to 25	0.20	1.33	0.07	0.35
0 to 15	0.16	0.83	0.06	0.22
0 to 10	0.13	0.67	0.05	0.17
0 to 4	0.13	0.10	0.04	0.05

As can be seen from the data, the peak-to-peak noise is 1.3 deg/hr as opposed to the predicted value of 0.8 to 1.0 deg/hr, and there is still sizeable motor-off to motor-on differences, especially in the larger bandwidths.

During the measurement of the peak-to-peak values on the oscilloscope, it was also observed that the noise signal was virtually sinusoidal in nature with a frequency of approximately 20 Hz. It was apparent that the gyro rate signal was being contaminated by test stand motion as noted in earlier tests, except that in this instance it had become a predominant factor due to the absence of the previously limiting wheel turbulence noise.

Figure 20 presents the PSD curve arrived at by computer analysis for the motor-on condition. This curve substantiates the relative effects of the 19 Hz seismic disturbance on the noise characteristics of the gyro. The rms noise arrived at by computer (the square root of the integral of the PSD curve) shows 0.39 deg/hr rms from 0 to 25 Hz, which is in close agreement with the data in Table VII. Further analysis of the computer output shows that the rms noise from 0 to 25 Hz would be 0.16 deg/hr if noise in the 18- to 20-Hz band were numerically filtered from the data. This 0.16 deg/hr rms noise would be equivalent to 0.96 deg/hr peak-to-peak over 25 Hz if the noise were truly random (a worst case analysis-- as the signal approaches a sine function the peak-to-peak to rms ratio diminishes from approximately 6:1 to 2.8:1).

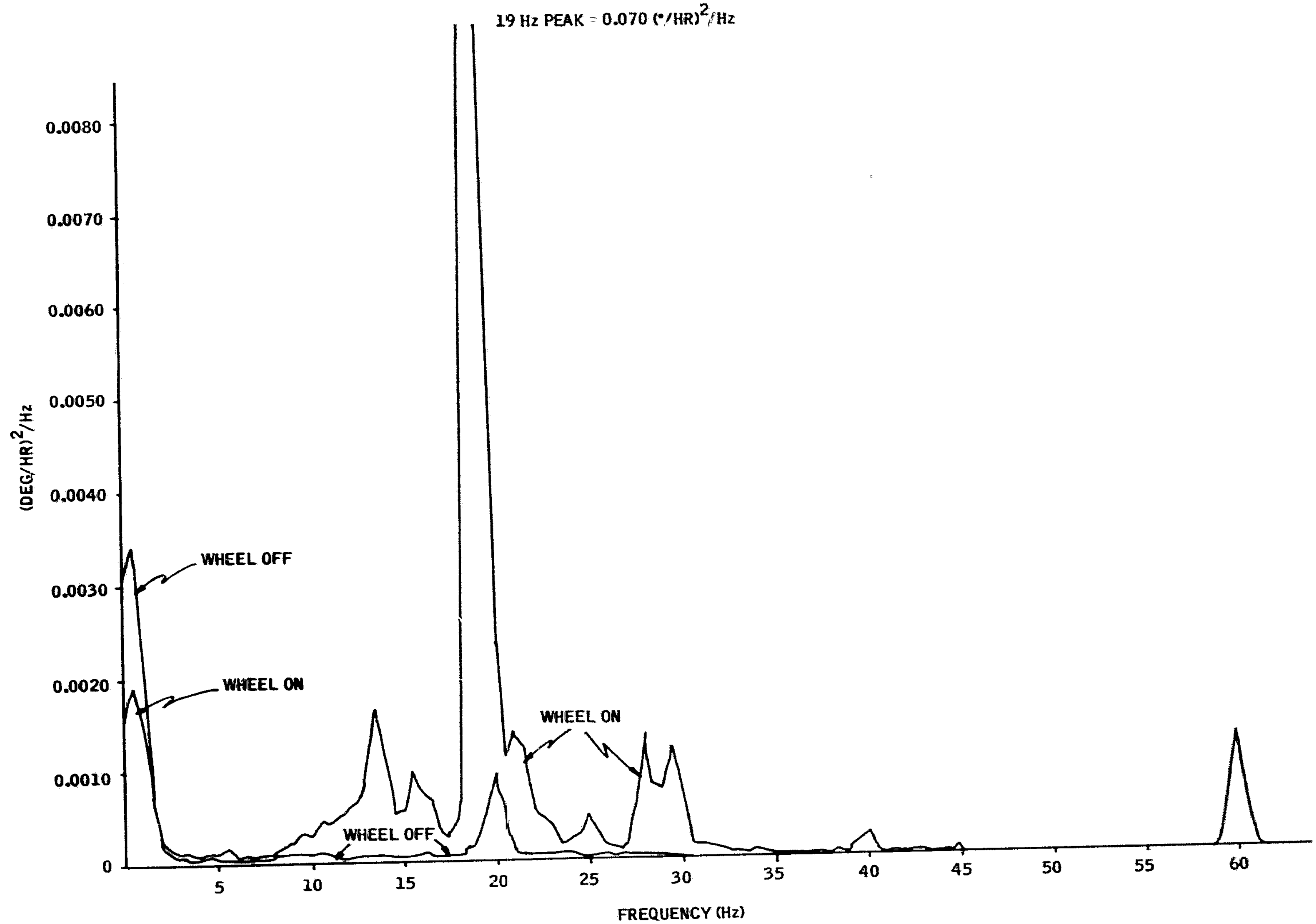

Figure 20. Power Spectral Density Low Noise GG334A Gyro 25 Hz Loop

Figure 20 also presents the PSD curve for the motor-off case. This curve explains the motor-on to motor-off difference as being primarily due to the influence of the 19-Hz sinusoidal component. From this motor-off PSD the rms noise to 25 Hz is 0.11 deg/hr, which compares realistically with the 0.16 deg/hr rms for motor-on after removal of the 19-Hz spike. In all 0 to 25 Hz measurements the rms levels obtained by computer are slightly larger than those obtained by the rms meter method (Table VII). This is due to the meter movements inability to measure below 1 Hz and the slight pickup in the 500-ft coaxial link to the computer used in obtaining the PSD data.

From this gyro test data it can be concluded that the incorporation of windage shrouds and the increase in angular momentum provided the capability of attaining the requirement of 1.0 deg/hr. Relative factors of improvement were 6X for wheel turbulence elimination and 2X for increased angular momentum. Secondly, with the noise levels achieved, measurements were hampered by the effects of test stand motion, and computer sampling and analysis must be used to obtain reliable estimates of gyro noise in lieu of transporting the gyro and the necessary peripheral equipment to seismically quiet areas. Figure 21 is a composite of the PSD curves of noise on the GG334A test vehicle before and after the elimination of wheel-induced turbulence. The data presented are from the motor-on cases of Figures 18 and 20 and serve to graphically summarize the level of noise reduction achieved on this program.

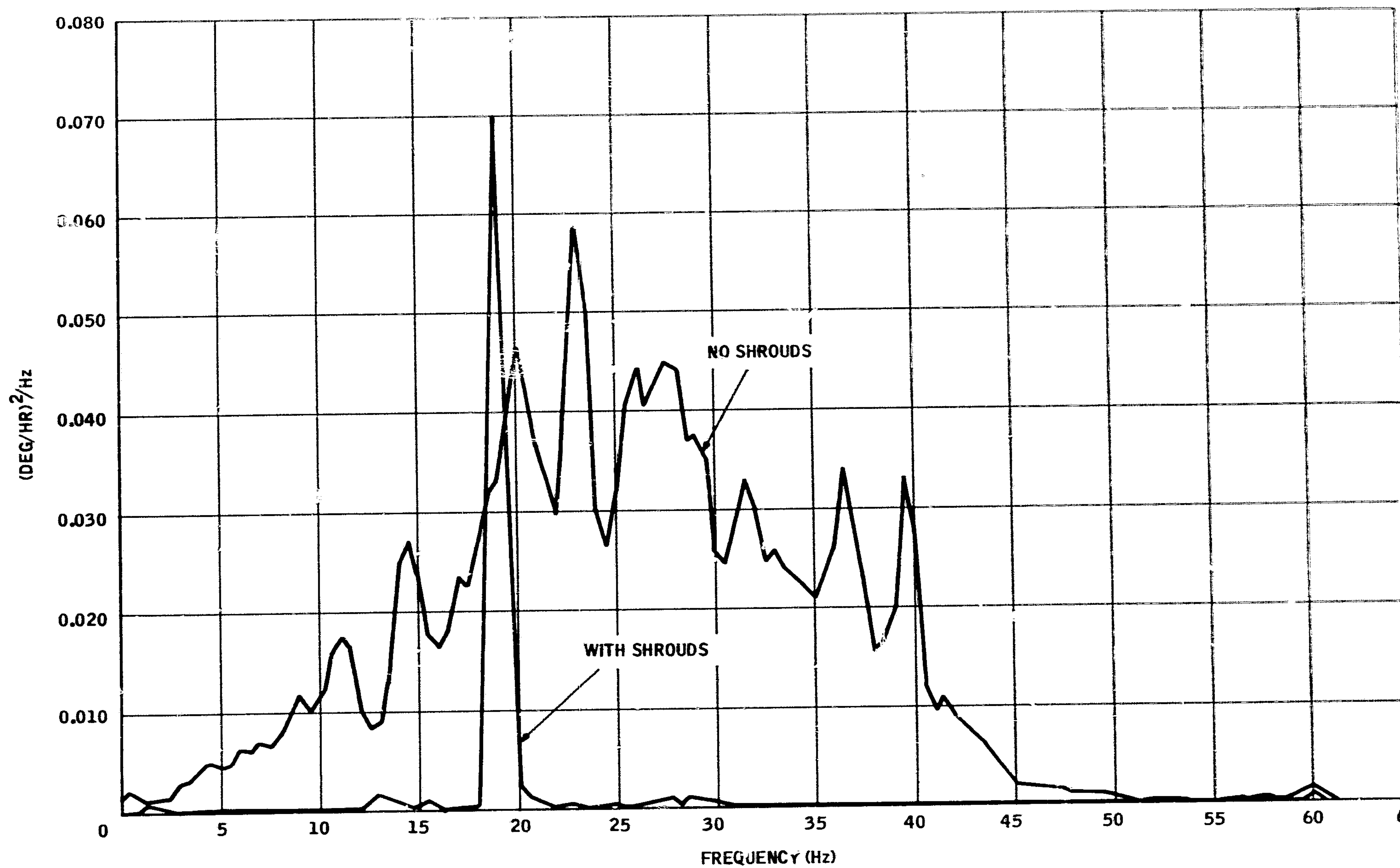

Figure 21. PSD GG334A Before and After Turbulence Elimination

SECTION IV
CONCLUSIONS

Conclusions reached on this program are that

- Low-frequency noise (0 to 25 Hz) on the output signal of the GG334S, GG159E, or GG334A type gyro is primarily caused by gas turbulence within the gimbal due to the rotating spinmotor.
- This turbulence can be virtually eliminated within the 24,000 rpm operating range of the spinmotor by the incorporation of suitably spaced windage shrouds resulting in laminar flow of gas in all regions of the gyro gimbal.
- Elimination of this turbulence produces at least a 6:1 reduction in gyro noise over the 0 to 25-Hz range, resulting in a GG334S gyro noise capability of 1.60 to 2.0 deg/hr peak-to-peak.
- Noise levels of less than 1.0 deg/hr on the GG334S type gyro can be achieved by an increase in angular momentum of 2X in addition to the elimination of turbulence.

In to these conclusions, the work accomplished under this program also served to establish the desirability of using large-scale models in the study of gas flow characteristics within gyro gimbals. This method allows detailed study of an otherwise confined volume both on a quantitative basis with anemometers and on a more sensitive qualitative basis with dye or smoke techniques. In addition, the usual experimental iterations take place on relatively inexpensive models as opposed to the actual gyro hardware.

The results of the testing on the low-noise gyro illustrate the need for use of PSD analysis of noise data. The use of rms voltmeters or oscilloscopes alone would not provide the necessary ability to isolate and mathematically treat the effects of rate inputs not pertinent to the study.

SECTION V
RECOMMENDATIONS

This study has shown that gyro noise can effectively be reduced by the incorporation of windage shrouds, as demonstrated on a modified GG334A gyro. Based on the results of this study, a gyro can be developed with low-noise requirements being considered as a design factor from the onset as with other gyro constraints such as torque stability, anisoelastic torque, aniso-inertia torque, and g-capability. Unlike the engineering gyro used in this program, it is possible that noise reduction techniques can be "designed in" so that existing gimbal and motor parts have dual functions, thereby eliminating the need for added piece parts and increased weight. A development effort exploring this possibility and culminating in the build and design proof test of a gyro would appear to be a meaningful extension of this effort.

With the noise reduction noted in this study, a test program could be initiated to determine the prime contributors to the remaining gyro noise. By necessity, any testing must include an assessment of the level of test stand motion in order to separate true gyro noise from rate input. This may best be accomplished by initial testing of a gyro at a known stable area by transportation of the gyro and test gear. At present, only the 19-Hz component has been identified as a test stand rate, and it is possible that other ranges of the spectrum may be influenced by this type of motion.

APPENDIX I

WINDAGE EFFECTS

Measurement and calculation indicate a gimbal volume of 50 cc. This indicates a mass of hydrogen of about 4.0×10^{-3} gm.

Hot-wire probe measurements inside the case with air indicate ubiquitous winds with mean speed of at least 5.0 ft/sec, with a rotor spin of 400 revolutions per second. Assuming the same speeds for hydrogen and further assuming that the gas revolves as a whole with that speed at the rotor radius, the angular momentum of the hydrogen is

$$H = 4.0 \times 10^{-3} \text{ gms} \times 5.0 \text{ ft/sec} \times 30.5 \text{ cm/ft} \times 1.5 \text{ cm}$$

$$= 0.9 \text{ gm-cm}^2/\text{sec}$$

Now assume that the direction of spin changes sinusoidally at some frequency ω with amplitude θ.

$$H = 0.9 \mu$$

$$\mu = \mu_o + \theta \sin \omega t \, N$$

Hence, torque $= \dot{H}$

$$= 0.9 \, \omega \, \theta \cos \omega t \, n$$

$$|H| = 0.9 \, \omega \, \theta$$

at 10 Hz, $\omega = 20 \pi$

$$|\dot{H}| = 19 \pi \theta$$

Thus, to produce

$$|\dot{H}| = 1 \text{ dyne-cm}$$

$$\theta = \left(\frac{1}{18 \pi} \right) \text{rad} \approx 1 \text{ deg}$$

Thus, a 1-deg variation in spin axis at a frequency of 10 Hz of the hydrogen assumed to be spinning as a solid body with 5 ft/sec speed at 1.5 cm radius would produce torques of 1.0 dyne-cm.

Another avenue of analysis is provided as follows. Consider the pumping of hydrogen by means of boundary layer effects on the rotating rotor. Let the rotor be idealized as a spinning sphere of radius 1.5 cm. Laminar boundary layer theory gives the windage torque on a sphere as

$$T = 3.27\, r^4 \sqrt{\rho \mu \omega^3}$$

where r is sphere radius

ρ is fluid density

μ is fluid viscosity

ω is sphere angular velocity

putting

$r = 1.5$ cm

$\mu = 87.6$ micropoise

$\rho = 0.00009$ gm/cc

$\omega = 400 \times 2\pi$ rad/sec

One gets

$T = 185.5$ dyne-cm

Although this torque is aligned with the spin axis (hence, not noticeable around the sensitive axis), it is easily seen that with such a large prime torque small fractions of this prime torque generated in orthogonal directions will easilv give 5 dyne-cm noise.

The major assumption of this spherical model lies in the value of r, since r is to the fourth power. If r be selected 1 cm instead of 1.5 cm, one would only get 36.0 dyne-cm torque. Since torque is rate of change of angular momentum, some 36.0 to 180 gm-cm^2/sec of angular momentum is being fed into the hydrogen in the case (because infeed equals rotor windage torque). This dissipates so rapidly that the steady value of hydrogen angular momentum is estimated at approximately 0.9 gm cm^2/sec. The time-average dissipation of spin-axis aligned angular momentum can only give spin-axis aligned (hence harmless) torques. But, as before, it is easy to image that there can be some slight transient rotations of the torque axis, which would be manifested as simultaneous generation of a torque on the gimbal and an equi-opposite torque imparted to the gas to change its spin axis.

APPENDIX II

SIMILARITY CALCULATIONS FOR LARGE MODEL

The flow around a rotating disk or cylinder is characterized by the Reynolds number

$$Rey = \frac{\rho V R}{\mu} = \frac{\rho \omega R^2}{\mu}$$

where

ρ = fluid density

μ = fluid viscosity

V = tangential velocity

R = radius

w = rotation (rad/sec)

The rotor in the GG334S gyro spins at 24, 000 rpm in hydrogen and has a radius of 0. 607 in. The density of hydrogen is $1.6.10^{-4}$ slugs/ft^3, and the viscosity is $1.83.10^{-7}$ $\frac{\text{slugs}}{\text{ft-sec}}$. The Reynolds number for these conditions is 5000.

To obtain a similar flow field in the four times scale model of the GG334S spinning in air which has a density of $2.34.10^{-3}$ slugs/ft^3 and a viscosity of $3.83.10^{-7}$ slugs/ft-sec, it is necessary to reduce the rotational speed in the model by a factor of

$$\frac{\omega_1}{\omega_2} = \frac{P_2 \mu_1}{P_1 \mu_2} \left(\frac{R_2}{R_1}\right)^2 = (14.5)\,(0.478)\,(16) = 111$$

For similar experiments with the large model in water, the rotational speed must be reduced by a factor of 940 to approximately 0. 4 rps.